Doctoral Dissertation

Development of the Preparation Methods of Biopolymer-Stabilized Metal Nanoparticles and Their Properties

（バイオポリマーで安定化された金属ナノ粒子の調製法の開発とその機能）

ASSAN Nazgul

July 2025

Graduate School of Engineering
The University of Osaka

Table of Contents

General Introduction

Metal nanoparticles as the main driving force of nanotechnology

Metal nanoparticles (Figure 1), particularly those of gold (Au) and platinum (Pt), have emerged as the main players in the advancement of nanotechnology due to their unique size-dependent properties, including enhanced catalytic activity, optical behavior, and surface reactivity.[1–3] Their exceptional performance has positioned them at the forefront of research across multiple scientific and technological domains. In recent decades, these nanoparticles have driven breakthroughs in catalysis,[4,5] biomedicine,[6–8] energy storage,[9,10] environmental science,[11,12] and materials engineering.[13] The ability to precisely control the structure and composition of metal nanoparticles at the nanoscale has enabled researchers to apply novel phenomena not observed in bulk materials,[14] reinforcing their pivotal role in shaping the future of these disciplines.

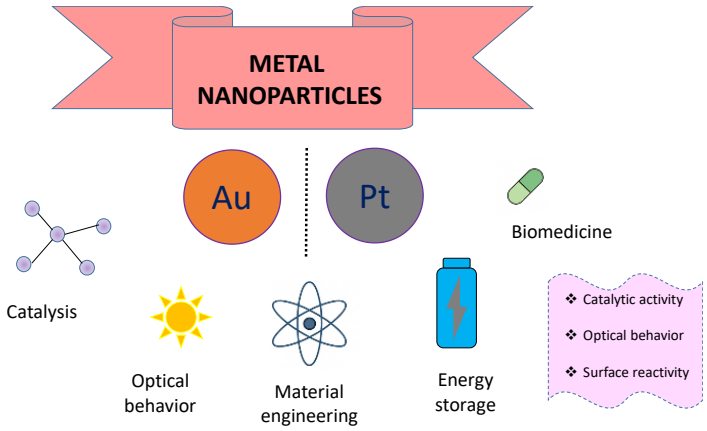

Figure 1 Metal Nanoparticles and their advantages

Beyond their vivid coloration derived from surface plasmon resonance, metal nanoparticles exhibit remarkable optical, catalytic, electronic, and physicochemical properties that emerge only when their size is reduced to a few nanometers.[15,16] Unlike their bulk counterparts, as shown for Au (Figure 2), which behave as continuous solids with predictable metallic properties, these nanoparticles (NPs) exhibit high surface-to-volume ratios,[17–19] quantum confinement effects,[20] and discrete electronic states.[21] These features endow them with exceptional reactivity in catalytic reactions, fine tunability of optical absorption, and other functionalities that make them uniquely suited for

applications ranging from photothermal therapies,[22,23] targeted drug delivery in biomedicine to high-sensitivity sensors,[24,25] energy storage devices,[9,26,27] and fine chemical synthesis in industrial settings.[28,29]

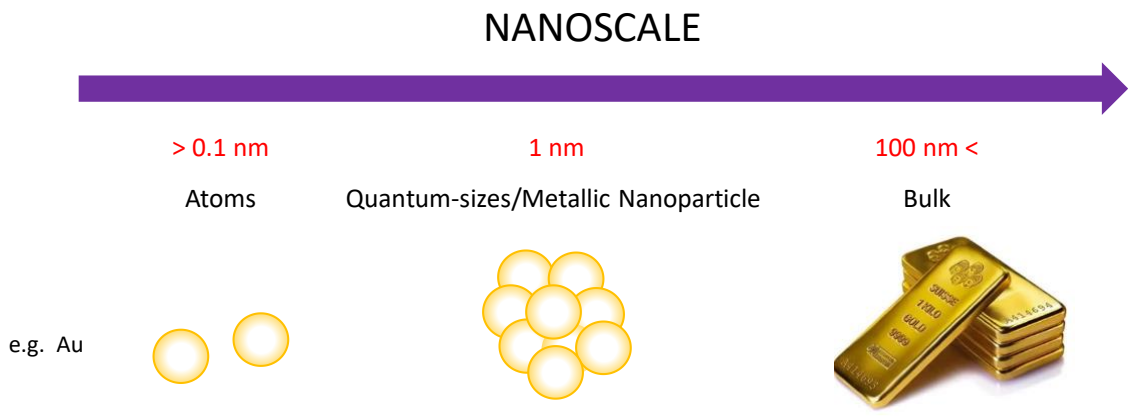

Figure 2 Size-Dependent Forms of Gold: From Atomic Scale to Bulk

Drawbacks of metal nanoparticles

Despite their immense potential, translating the unique properties of metal nanoparticles into practical applications remains a significant challenge.[30,31] Producing nanoparticles (Figure 3) with precisely controlled size, shape, crystalline structure, surface charge, stability, and uniform dispersion is a critical prerequisite. This is significant because even slight deviations in these parameters can render them ineffective or dramatically alter their performance in target applications.[32–34] For example, in catalysis, the activity and selectivity of metal nanoparticles are often highly size-dependent, with subtle differences in diameter leading to dramatic changes in reaction pathways or product distributions.[35,36] In photothermal therapies, the efficacy of nanoparticles in converting light into localized heat for destroying cancer cells depends sensitively on their shape and size, which determine their optical absorption and scattering cross-sections.[37–39] In sensors, the sensitivity and reproducibility of detection are influenced by how uniformly the nanoparticles are dispersed on substrates or in solution.[40,41] These strict needs have led to intense efforts to create reliable and adjustable methods for them.

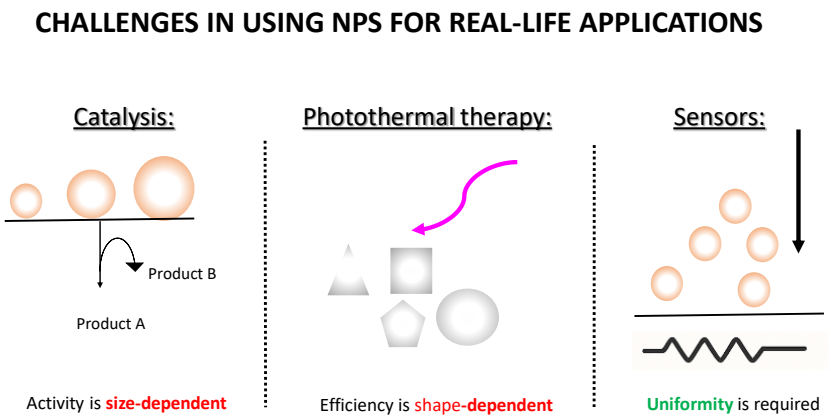

Figure 3 Critical parameters affecting NP performance in real-world applications

Methods of preparation of metal nanoparticles

Historically, the synthesis of metal nanoparticles (Figure 4) has been dominated by chemical and physical routes that often involve strong reducing agents such as sodium borohydride,[42] hydrazine,[43] or citrate,[44] elevated temperatures,[45] highly acidic or basic pH conditions,[46,47] and the use of surfactants[48] or capping agents[49] to control growth and prevent agglomeration.[50] While these methods have produced significant breakthroughs and contributed enormously to our understanding of nanoparticle science, they come with significant limitations. The strong reducing agents can generate hazardous byproducts,[51,52] the high temperatures and extreme pH conditions can lead to environmental hazards and restrict the types of materials that can be used as stabilizing matrices,[31,53–55] and the presence of surfactants or organic stabilizers often introduces impurities that may need to be removed or that can compromise the functionality of the final nanocomposite, especially in sensitive biomedical applications.[48,56,57] Additionally, these methods often suffer from challenges in scalability, reproducibility, and fine control over nanoparticle morphology, which is critical for tailoring their properties to specific applications. [58,59]

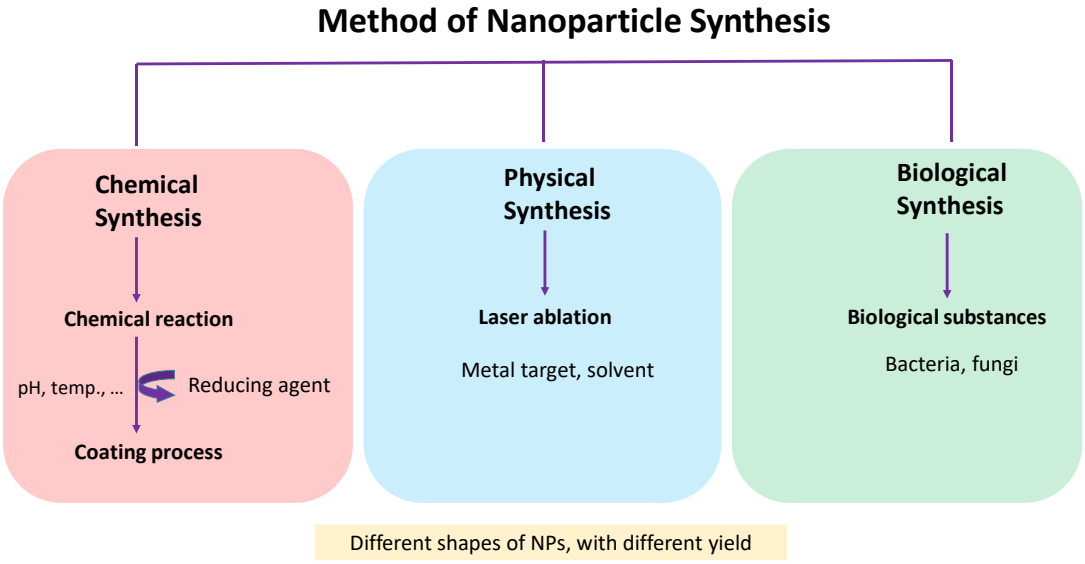

Figure 4 Overview of nanoparticle synthetic methods.

Biopolymers as green stabilizers for metal nanoparticle synthesis

As global awareness of environmental sustainability and the need for safer, more biocompatible materials has increased, researchers have turned their attention to greener and more benign synthesis strategies for the production of metal nanoparticles.[60–62] Among these, the use of biopolymers (Figure 5) as stabilizing matrices has emerged as a particularly promising direction. Biopolymers such as chitosan, gelatin, and collagen are abundant, renewable, biodegradable, and often exhibit excellent compatibility with biological systems.[63,64] They possess a rich array of functional groups, such as hydroxyl, amino, and carboxyl.[65–68] These groups usually interact easily with metal ions or growing nanoparticle surfaces through coordination bonds, hydrogen bonding, electrostatic interactions, or non-covalent forces. These features make biopolymers not only appropriate stabilizers that prevent aggregation and growth beyond the nanoscale but also active participants that can direct nucleation, influence growth pathways, and mediate the assembly of nanoparticles into higher-order structures. This can potentially impart additional functionalities or biological affinities to the resulting nanocomposites.[69–71]

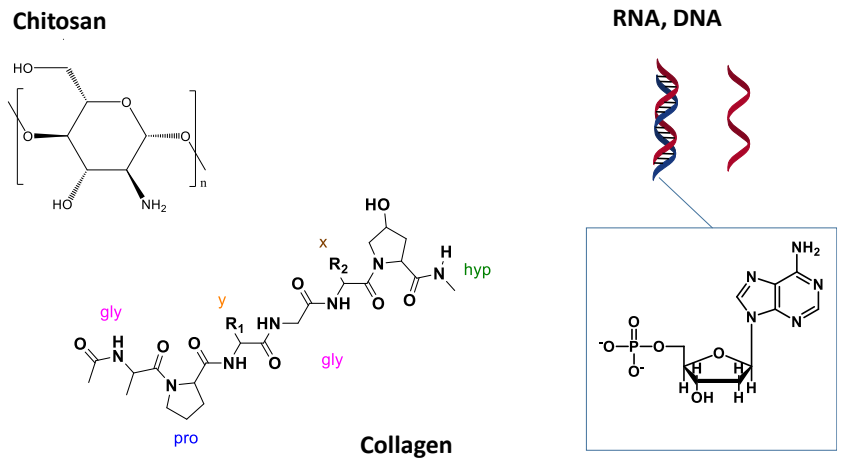

Figure 5 Molecular structures of representative biopolymers used in nanomaterial synthesis

Challenges in integrating metal nanoparticles into biopolymer matrices

Yet, despite their promise, incorporating metal nanoparticles into biopolymer matrices is not a straightforward process. Biopolymers are, by their nature, often chemically sensitive and structurally fragile. Their native secondary, tertiary, or even quaternary structures can be disrupted by the heat, extreme pH, or strong reducing conditions that are typically employed in conventional nanoparticle syntheses. In the case of chitosan, gelatin, and collagen, such conditions can lead to irreversible denaturation, partial hydrolysis, uncontrolled degradation, or dissolution.[63,71–74] These structural changes not only undermine the mechanical integrity of the biopolymer matrix but also compromise the very functionalities such as bioactivity, cell adhesion motifs, or selective permeability, which is one of the most attractive points of these materials. Moreover, the thermal or chemical stresses applied during nanoparticle synthesis can induce unwanted crosslinking or rearrangement of the polymer chains, leading to heterogeneous materials with unpredictable or poorly reproducible properties.[75,76]

Another major challenge lies in the use of surfactants or other organic stabilizers that are often necessary in conventional approaches to prevent nanoparticle aggregation and control size distribution. While effective in stabilizing metal colloids, these additives may remain in the final product, introducing potential cytotoxicity in biomedical applications,[48] altering surface chemistry in undesirable ways, or interfering with subsequent functionalization or bioconjugation steps.[77,78] Removing these residual stabilizers often

requires additional purification steps, which can be time-consuming, costly, and not always entirely effective, especially when working at the nanoscale.

Furthermore, controlling the size, distribution, and dispersion of nanoparticles within dense or viscous biopolymer matrices presents additional complexities. Biopolymers such as collagen naturally form rigid, hydrated networks with significant steric hindrance and constrained diffusion pathways.[79] Embedding nanoparticles within such matrices in a uniform manner, without aggregation or clustering, requires careful control over reaction kinetics, local concentration gradients, and the interplay between matrix dynamics and nanoparticle nucleation and growth processes.[80,81] Any lack of uniformity or reproducibility in this process can lead to batch-to-batch variations in mechanical, optical, or catalytic properties of the resulting composites, undermining their utility in practical applications [82]

Integrating metal nanoparticles into biopolymer matrices poses a significant challenge due to the fragile nature of biopolymers such as chitosan, gelatin, and collagen. Traditional synthesis methods often involve harsh conditions that can damage these materials. To overcome this, researchers are developing milder and greener approaches that use the functional groups in biopolymers to control nanoparticle formation. These biopolymers not only stabilize the nanoparticles but also influence their growth and assembly. Solving these challenges is an important factor to creating safe, sustainable nanomaterials for use in medicine, catalysis, and environmental technologies.

Thesis Outline

This PhD work (Figure 6) was motivated by the need to address critical challenges in the synthesis of biopolymer-stabilized metal nanoparticles by developing three complementary, structurally mild, and environmentally benign approaches. Each strategy is grounded in a distinct physicochemical principle, and collectively, they constitute a coherent framework for embedding metal nanoparticles into soft biomaterials while preserving, or even enhancing, their structural and functional integrity.

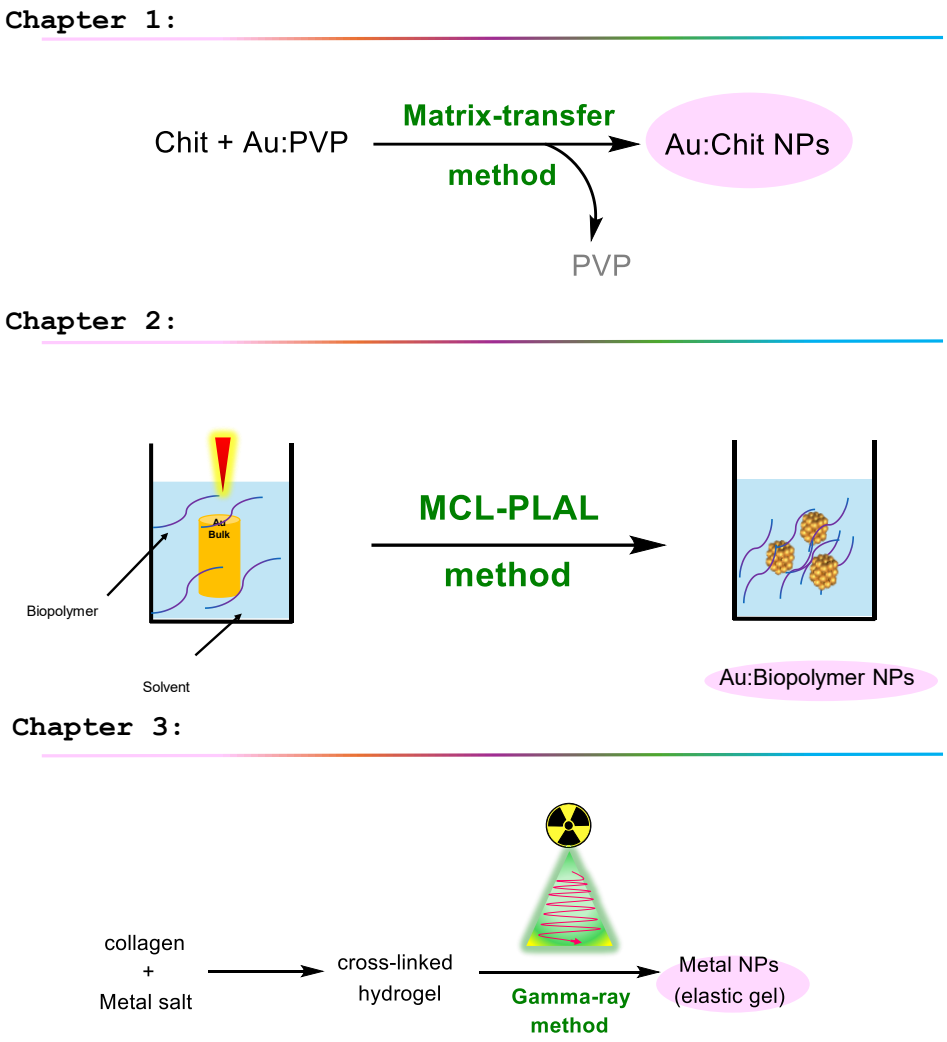

Figure 6 Outline of this thesis work

Chapter 1 presents a matrix-transfer approach for synthesis of size-selective gold nanoparticles stabilized by chitosan. Gold nanoparticles with diameters ranging from 1 to 6 nm were first synthesized in a polyvinylpyrrolidone (PVP) matrix using established reduction or seed-mediated growth protocols. These gold-PVP composites were then subjected to an interfacial transfer process, moving the nanoparticles from the PVP phase into a chitosan matrix using a carefully designed biphasic solvent system. This procedure effectively preserved the nanoparticle size and prevented agglomeration, producing a new class of chitosan-stabilized gold nanocomposites. Importantly, catalytic studies revealed that these materials display high activity in the homocoupling of phenylboronic acid and

that the catalytic selectivity and efficiency are strongly size-dependent, thus highlighting both the robustness of the synthesis method and the active role of the chitosan matrix.

Chapter 2 explores pulsed laser ablation in liquid (PLAL) using microchip laser (MCL) as a green, additive-free method to directly embed nanoparticles into biopolymer solutions. Unlike conventional PLAL techniques, which typically require high-power lasers and may damage sensitive biomatrices, the use of a compact microchip laser with low pulse energy and short pulse duration allows efficient ablation with minimal thermal damage. When applied to gelatin matrices, this method produced well-dispersed gold nanoparticles approximately 4 nm in size, while in collagen suspensions, nanoparticles around 2.4 nm were formed in the supernatant without significant denaturation of the biomatrix. Spectroscopic measurements confirmed that the secondary structures of gelatin and collagen were preserved mainly, and in some cases subtly modulated, suggesting potential for tailoring bioactivity. This approach offers a powerful pathway for producing biocompatible, nanoparticle-loaded matrices with potential applications in drug delivery, imaging, and minimally invasive therapies.

Chapter 3 introduces a radiochemical reduction approach using gamma-ray irradiation from a ^{60}Co (cobalt-60) source to induce nanoparticle formation in situ within collagen gels. In this method, type I collagen solutions containing dissolved metal precursors such as gold or platinum salts were first pre-gelled and then exposed to gamma irradiation, which induced water radiolysis. The resulting reactive species simultaneously reduced the metal ions to nanoparticles and triggered additional crosslinking within the collagen network. The result was a class of collagen-based metal nanocomposite hydrogels with uniformly dispersed nanoparticles and significantly enhanced mechanical stiffness up to five times higher than the precursor hydrogels. These new materials also displayed reversible photothermal responses under UV-visible light, expanding their potential utility as photothermal actuators, sensors, or tissue scaffold materials with built-in stimuli responsiveness.

Although each method stems from distinct scientific questions and experimental designs, the approaches exhibit significant synergy. All three approaches avoid harsh reducing agents, high temperatures, and toxic surfactants, advancing the principles of green

chemistry. Each method uniquely addresses core challenges: precise nanoparticle size control (matrix-transfer), gentle incorporation into fragile matrices (MCL–PLAL), and mechanical reinforcement with responsive behavior (radiochemical approach). Together, these strategies enable the rational design of soft-material nanocomposites with tunable mechanical, catalytic, or bioresponsive properties. Such materials hold promises not only in catalysis, where size-dependent activity can be applied for greener transformations, but also in biomedicine, where precise control over nanoparticle distribution and matrix compatibility is crucial for safety and efficacy. In materials engineering, the interplay between mechanical robustness and responsiveness to external stimuli opens new avenues for sensors, actuators, and adaptive scaffold systems.[83]

References

(1) Yamada, M.; Foote, M.; Prow, T. W. Therapeutic Gold, Silver, and Platinum Nanoparticles. *Wiley Interdiscip. Rev. Nanomedicine Nanobiotechnology* **2015**, *7* (3), 428–445. https://doi.org/10.1002/wnan.1322.

(2) Yaqoob, S. B.; Adnan, R.; Rameez Khan, R. M.; Rashid, M. Gold, Silver, and Palladium Nanoparticles: A Chemical Tool for Biomedical Applications. *Front. Chem.* **2020**, *8* (June), 1–15. https://doi.org/10.3389/fchem.2020.00376.

(3) Gutiérrez de la Rosa, S. Y.; Muñiz Diaz, R.; Villalobos Gutiérrez, P. T.; Patakfalvi, R.; Gutiérrez Coronado, Ó. Functionalized Platinum Nanoparticles with Biomedical Applications. *Int. J. Mol. Sci.* **2022**, *23* (16). https://doi.org/10.3390/ijms23169404.

(4) Baruwa, A.; Gbadeyan, O. J.; Permaul, K. Revolutionizing Biotechnology: The Impact of Nanocatalysts and Nanomaterials—a Comprehensive Review. *Discov. Mater.* **2025**, *5* (1). https://doi.org/10.1007/s43939-025-00269-9.

(5) Astruc, D. Introduction: Nanoparticles in Catalysis. *Chem. Rev.* **2020**, *120* (2), 461–463. https://doi.org/10.1021/acs.chemrev.8b00696.

(6) Silva, D. F.; Melo, A. L. P.; Uchôa, A. F. C.; Pereira, G. M. A.; Alves, A. E. F.; Vasconcellos, M. C.; Xavier-Júnior, F. H.; Passos, M. F. Biomedical Approach of Nanotechnology and Biological Risks: A Mini-Review. *Int. J. Mol. Sci.* **2023**, *24* (23). https://doi.org/10.3390/ijms242316719.

(7) Haleem, A.; Javaid, M.; Singh, R. P.; Rab, S.; Suman, R. Applications of Nanotechnology in Medical Field: A Brief Review. *Glob. Heal. J.* **2023**, *7* (2), 70–77. https://doi.org/10.1016/j.glohj.2023.02.008.

(8) Ma, X.; Tian, Y.; Yang, R.; Wang, H.; Allahou, L. W.; Chang, J.; Williams, G.; Knowles, J. C.; Poma, A. Nanotechnology in Healthcare, and Its Safety and Environmental Risks. *J. Nanobiotechnology* **2024**, *22* (1). https://doi.org/10.1186/s12951-024-02901-x.

(9) Mohammed, H.; Mia, F.; Wiggins, J.; Desai, S. Nanomaterials for Energy Storage Systems — A Review. **2025**.

(10) Nanotechnology for Electrochemical Energy Storage. *Nat. Nanotechnol.* **2023**, *18* (10), 1117. https://doi.org/10.1038/s41565-023-01529-6.

(11) Pranabesh Ghosh, Abhishek Konar, Sunanda Halder, Shivaranjani DS, J. K. Impact of Nanotechnology on Environment – A Review. *Environ. Sci. Arch.* **2024**, *3* (1), 152–163. https://doi.org/10.5281/zenodo.10963714.

(12) Del Prado-Audelo, M. L.; García Kerdan, I.; Escutia-Guadarrama, L.; Reyna-González, J. M.; Magaña, J. J.; Leyva-Gómez, G. Nanoremediation: Nanomaterials and Nanotechnologies for Environmental Cleanup. *Front. Environ. Sci.* **2021**, *9* (December), 1–7. https://doi.org/10.3389/fenvs.2021.793765.

(13) Ankita Saroha. The Role of Nanotechnology in Electronic Properties of Materials. *Univers. Res. Reports* **2024**, *11* (5), 10–15. https://doi.org/https://doi.org10.36676/urr.v11.i5.1444.

(14) Mekuye, B.; Abera, B. Nanomaterials: An Overview of Synthesis, Classification, Characterization, and Applications. *Nano Sel.* **2023**, *4* (8), 486–501. https://doi.org/10.1002/nano.202300038.

(15) Su, Y. H.; Ke, Y. F.; Cai, S. L.; Yao, Q. Y. Surface Plasmon Resonance of Layer-by-Layer Gold Nanoparticles Induced Photoelectric Current in Environmentally-Friendly Plasmon-

Sensitized Solar Cell. *Light Sci. Appl.* **2012**, *1* (JUNE), 2–6. https://doi.org/10.1038/lsa.2012.14.

(16) Kunwar, S.; Sui, M.; Pandey, P.; Gu, Z.; Pandit, S.; Lee, J. Improved Configuration and LSPR Response of Platinum Nanoparticles via Enhanced Solid State Dewetting of In-Pt Bilayers. *Sci. Rep.* **2019**, *9* (1), 1–14. https://doi.org/10.1038/s41598-018-37849-0.

(17) Mourdikoudis, S.; Pallares, R. M.; Thanh, N. T. K. Characterization Techniques for Nanoparticles: Comparison and Complementarity upon Studying Nanoparticle Properties. *Nanoscale* **2018**, *10* (27), 12871–12934. https://doi.org/10.1039/c8nr02278j.

(18) Joudeh, N.; Linke, D. Nanoparticle Classification, Physicochemical Properties, Characterization, and Applications: A Comprehensive Review for Biologists. *J. Nanobiotechnology* **2022**, *20* (1), 1–29. https://doi.org/10.1186/s12951-022-01477-8.

(19) Pozzi, M.; Jonak Dutta, S.; Kuntze, M.; Bading, J.; Rüßbült, J. S.; Fabig, C.; Langfeldt, M.; Schulz, F.; Horcajada, P.; Parak, W. J. Visualization of the High Surface-to-Volume Ratio of Nanomaterials and Its Consequences. *J. Chem. Educ.* **2024**, *101* (8), 3146–3155. https://doi.org/10.1021/acs.jchemed.4c00089.

(20) Blackman, G. N.; Genov, D. A. Bounds on Quantum Confinement Effects in Metal Nanoparticles. *Phys. Rev. B* **2018**, *97* (11), 1–10. https://doi.org/10.1103/PhysRevB.97.115440.

(21) Jin, R.; Higaki, T. Open Questions on the Transition between Nanoscale and Bulk Properties of Metals. *Commun. Chem.* **2021**, *4* (1), 6–9. https://doi.org/10.1038/s42004-021-00466-6.

(22) Prabhakaran, P.; Kumar, P.; Lim, D. Photothermal Effect of Gold Nanoparticles as a Nanomedicine for Diagnosis and Therapeutics. **2023**, 2349.

(23) Yu, S.; Xia, G.; Yang, N.; Yuan, L.; Li, J.; Wang, Q.; Li, D.; Ding, L.; Fan, Z.; Li, J. Noble Metal Nanoparticle-Based Photothermal Therapy: Development and Application in Effective Cancer Therapy. *Int. J. Mol. Sci.* **2024**, *25* (11), 5632. https://doi.org/10.3390/ijms25115632.

(24) Roshani, M.; Rezaian-Isfahni, A.; Lotfalizadeh, M. H.; Khassafi, N.; Abadi, M. H. J. N.; Nejati, M. Metal Nanoparticles as a Potential Technique for the Diagnosis and Treatment of Gastrointestinal Cancer: A Comprehensive Review. *Cancer Cell Int.* **2023**, *23* (1), 1–23. https://doi.org/10.1186/s12935-023-03115-1.

(25) Georgeous, J.; AlSawaftah, N.; Abuwatfa, W. H.; Husseini, G. A. Review of Gold Nanoparticles: Synthesis, Properties, Shapes, Cellular Uptake, Targeting, Release Mechanisms and Applications in Drug Delivery and Therapy. *Pharmaceutics* **2024**, *16* (10). https://doi.org/10.3390/pharmaceutics16101332.

(26) Yang, G.; Hu, L.; Keiper, T. D.; Xiong, P.; Hallinan, D. T. Gold Nanoparticle Monolayers with Tunable Optical and Electrical Properties. *Langmuir* **2016**, *32* (16), 4022–4033. https://doi.org/10.1021/acs.langmuir.6b00347.

(27) Salaheldeen, M.; M. Abu-Dief, A.; El-Dabea, T. Functionalization of Nanomaterials for Energy Storage and Hydrogen Production Applications. *Materials (Basel).* **2025**, *18* (4). https://doi.org/10.3390/ma18040768.

(28) Zhao, J.; Wang, J.; Brock, A. J.; Zhu, H. Plasmonic Heterogeneous Catalysis for Organic Transformations. *J. Photochem. Photobiol. C Photochem. Rev.* **2022**, *52* (February), 100539. https://doi.org/10.1016/j.jphotochemrev.2022.100539.

(29) Patel, R. Journal of Materials Science and Nanomaterials The Role of Nanomaterials in Catalysis : Mechanisms and Applications. *J Mater Sci Nanomater* **2024**, *8* (2). https://doi.org/10.4172/jmsn.100123.

(30) Desai, N. Challenges in Development of Nanoparticle-Based Therapeutics. *AAPS J.* **2012**, *14* (2), 282–295. https://doi.org/10.1208/s12248-012-9339-4.

(31) Altammar, K. A. A Review on Nanoparticles: Characteristics, Synthesis, Applications, and Challenges. *Front. Microbiol.* **2023**, *14* (April), 1–20. https://doi.org/10.3389/fmicb.2023.1155622.

(32) Vreeland, E. C.; Watt, J.; Schober, G. B.; Hance, B. G.; Austin, M. J.; Price, A. D.; Fellows, B. D.; Monson, T. C.; Hudak, N. S.; Maldonado-Camargo, L.; Bohorquez, A. C.; Rinaldi, C.; Huber, D. L. Enhanced Nanoparticle Size Control by Extending LaMer's Mechanism. *Chem. Mater.* **2015**, *27* (17), 6059–6066. https://doi.org/10.1021/acs.chemmater.5b02510.

(33) Xie, W.; Guo, Z.; Gao, F.; Gao, Q.; Wang, D.; Liaw, B. S.; Cai, Q.; Sun, X.; Wang, X.; Zhao, L. Shape-, Size-and Structure-Controlled Synthesis and Biocompatibility of Iron Oxide Nanoparticles for Magnetic Theranostics. *Theranostics* **2018**, *8* (12), 3284–3307. https://doi.org/10.7150/thno.25220.

(34) Arno, M. C.; Inam, M.; Weems, A. C.; Li, Z.; Binch, A. L. A.; Platt, C. I.; Richardson, S. M.; Hoyland, J. A.; Dove, A. P.; O'Reilly, R. K. Exploiting the Role of Nanoparticle Shape in Enhancing Hydrogel Adhesive and Mechanical Properties. *Nat. Commun.* **2020**, *11* (1). https://doi.org/10.1038/s41467-020-15206-y.

(35) An, K.; Somorjai, G. A. Size and Shape Control of Metal Nanoparticles for Reaction Selectivity in Catalysis. *ChemCatChem* **2012**, *4* (10), 1512–1524. https://doi.org/10.1002/cctc.201200229.

(36) Dong, C.; Lian, C.; Hu, S.; Deng, Z.; Gong, J.; Li, M.; Liu, H.; Xing, M.; Zhang, J. Size-Dependent Activity and Selectivity of Carbon Dioxide Photocatalytic Reduction over Platinum Nanoparticles. *Nat. Commun.* **2018**, *9* (1), 1–11. https://doi.org/10.1038/s41467-018-03666-2.

(37) Pattani, V. P.; Tunnell, J. W. Nanoparticle-Mediated Photothermal Therapy: A Comparative Study of Heating for Different Particle Types. *Lasers Surg. Med.* **2012**, *44* (8), 675–684. https://doi.org/10.1002/lsm.22072.

(38) Vikas; Kumar, R.; Soni, S. Concentration-Dependent Photothermal Conversion Efficiency of Gold Nanoparticles under near-Infrared Laser and Broadband Irradiation. *Beilstein J. Nanotechnol.* **2023**, *14*, 205–217. https://doi.org/10.3762/bjnano.14.20.

(39) Eladarousy, O.; Zibara, Z.; Hussari, K.; Al Helou, N.; Nicolas, R. Optimizing Plasmonic Photothermal Therapy a Numerical Study on Tissue Specific Thermal and Optical Properties for Cancer Treatment. *Sci. Rep.* **2025**, *15* (1), 1–11. https://doi.org/10.1038/s41598-025-95798-x.

(40) Hwang, J. S.; Yang, M. Sensitive and Reproducible Gold SERS Sensor Based on Interference Lithography and Electrophoretic Deposition. *Sensors (Switzerland)* **2018**, *18* (11). https://doi.org/10.3390/s18114076.

(41) Mansour, E.; Sherbo, S.; Saliba, W.; Kloper, V.; Haick, H. Effect of the Dispersion Process and Nanoparticle Quality on Chemical Sensing Performance. *ACS Omega* **2022**, *7* (26), 22484–22491. https://doi.org/10.1021/acsomega.2c01668.

(42) Deraedt, C.; Salmon, L.; Gatard, S.; Ciganda, R.; Hernandez, R.; Mayor, M.; Astruc, D.

Sodium Borohydride Stabilizes Very Active Gold Nanoparticle Catalysts. *Chem. Commun.* **2012**, *50* (91), 14194–14196. https://doi.org/10.1039/c4cc05946h.

(43) Wang, Y.; Shi, Y. F.; Chen, Y. B.; Wu, L. M. Hydrazine Reduction of Metal Ions to Porous Submicro-Structures of Ag, Pd, Cu, Ni, and Bi. *J. Solid State Chem.* **2012**, *191*, 19–26. https://doi.org/10.1016/j.jssc.2012.02.059.

(44) Wuithschick, M.; Birnbaum, A.; Witte, S.; Sztucki, M.; Vainio, U.; Pinna, N.; Rademann, K.; Emmerling, F.; Kraehnert, R.; Polte, J. Turkevich in New Robes: Key Questions Answered for the Most Common Gold Nanoparticle Synthesis. *ACS Nano* **2015**, *9* (7), 7052–7071. https://doi.org/10.1021/acsnano.5b01579.

(45) Mountrichas, G.; Pispas, S.; Kamitsos, E. I. Effect of Temperature on the Direct Synthesis of Gold Nanoparticles Mediated by Poly(Dimethylaminoethyl Methacrylate) Homopolymer. *J. Phys. Chem. C* **2014**, *118* (39), 22754–22759. https://doi.org/10.1021/jp505725v.

(46) Marciniak, L.; Nowak, M.; Trojanowska, A.; Tylkowski, B.; Jastrzab, R. The Effect of Ph on the Size of Silver Nanoparticles Obtained in the Reduction Reaction with Citric and Malic Acids. *Materials (Basel).* **2020**, *13* (23), 1–12. https://doi.org/10.3390/ma13235444.

(47) Alqadi, M. K.; Abo Noqtah, O. A.; Alzoubi, F. Y.; Alzouby, J.; Aljarrah, K. PH Effect on the Aggregation of Silver Nanoparticles Synthesized by Chemical Reduction. *Mater. Sci. Pol.* **2014**, *32* (1), 107–111. https://doi.org/10.2478/s13536-013-0166-9.

(48) Miyazawa, T.; Itaya, M.; Burdeos, G. C.; Nakagawa, K.; Miyazawa, T. A Critical Review of the Use of Surfactant-Coated Nanoparticles in Nanomedicine and Food Nanotechnology. *Int. J. Nanomedicine* **2021**, *16*, 3937–3999. https://doi.org/10.2147/IJN.S298606.

(49) Javed, R.; Zia, M.; Naz, S.; Aisida, S. O.; Ain, N. ul; Ao, Q. Role of Capping Agents in the Application of Nanoparticles in Biomedicine and Environmental Remediation: Recent Trends and Future Prospects. *J. Nanobiotechnology* **2020**, *18* (1), 1–15. https://doi.org/10.1186/s12951-020-00704-4.

(50) Wayman, T. M. R.; Lomonosov, V.; Ringe, E. Capping Agents Enable Well-Dispersed and Colloidally Stable Metallic Magnesium Nanoparticles. *J. Phys. Chem. C* **2024**, *128* (11), 4666–4676. https://doi.org/10.1021/acs.jpcc.4c00366.

(51) Fahim, M.; Shahzaib, A.; Nishat, N.; Jahan, A.; Bhat, T. A.; Inam, A. Green Synthesis of Silver Nanoparticles: A Comprehensive Review of Methods, Influencing Factors, and Applications. *JCIS Open* **2024**, *16* (October), 100125. https://doi.org/10.1016/j.jciso.2024.100125.

(52) Joudeh, N.; Saragliadis, A.; Koster, G.; Mikheenko, P.; Linke, D. Synthesis Methods and Applications of Palladium Nanoparticles: A Review. *Front. Nanotechnol.* **2022**, *4* (November), 1–24. https://doi.org/10.3389/fnano.2022.1062608.

(53) dos Santos, O. A. L.; Pizzorno Backx, B.; Abumousa, R. A.; Bououdina, M. Environmental Implications Associated with the Development of Nanotechnology: From Synthesis to Disposal. *Nanomaterials* **2022**, *12* (23). https://doi.org/10.3390/nano12234319.

(54) Singh, H.; Desimone, M. F.; Pandya, S.; Jasani, S.; George, N.; Adnan, M.; Aldarhami, A.; Bazaid, A. S.; Alderhami, S. A. Revisiting the Green Synthesis of Nanoparticles: Uncovering Influences of Plant Extracts as Reducing Agents for Enhanced Synthesis Efficiency and Its Biomedical Applications. *Int. J. Nanomedicine* **2023**, *18* (August),

4727–4750. https://doi.org/10.2147/IJN.S419369.

(55) Chopada, R.; Sarwate, R.; Kumar, V. Effect of Mild to Extreme PH, Temperature, and Ionic Strength on the Colloidal Stability of Differentially Capped Gold Nanoparticles. *J. Mol. Struct.* **2025**, *1323* (November 2024), 140751. https://doi.org/10.1016/j.molstruc.2024.140751.

(56) Stolaś, A.; Darmadi, I.; Nugroho, F. A. A.; Moth-Poulsen, K.; Langhammer, C. Impact of Surfactants and Stabilizers on Palladium Nanoparticle–Hydrogen Interaction Kinetics: Implications for Hydrogen Sensors. *ACS Appl. Nano Mater.* **2020**, *3* (3), 2647–2653. https://doi.org/10.1021/acsanm.0c00020.

(57) Cortés, H.; Hernández-Parra, H.; Bernal-Chávez, S. A.; Del Prado-Audelo, M. L.; Caballero-Florán, I. H.; Borbolla-Jiménez, F. V.; González-Torres, M.; Magaña, J. J.; Leyva-Gómez, G. Non-Ionic Surfactants for Stabilization of Polymeric Nanoparticles for Biomedical Uses. *Materials (Basel).* **2021**, *14* (12). https://doi.org/10.3390/ma14123197.

(58) Paliwal, R.; Babu, R. J.; Palakurthi, S. Nanomedicine Scale-up Technologies: Feasibilities and Challenges. *Ageing Int.* **2014**, *15* (6), 1527–1534. https://doi.org/10.1208/s12249-014-0177-9.

(59) Andresen, E.; Islam, F.; Prinz, C.; Gehrmann, P.; Licha, K.; Roik, J.; Recknagel, S.; Resch-Genger, U. Assessing the Reproducibility and Up-Scaling of the Synthesis of Er,Yb-Doped NaYF4-Based Upconverting Nanoparticles and Control of Size, Morphology, and Optical Properties. *Sci. Rep.* **2023**, *13* (1), 1–13. https://doi.org/10.1038/s41598-023-28875-8.

(60) Patra, J. M.; Panda, S. S.; Dhal, N. K. A Review on Green Synthesis of Gold Nanoparticles. *Int. J. Pharma Bio Sci.* **2015**, *6* (3), P251–P261. https://doi.org/10.1016/j.scca.2025.100071.

(61) Radulescu, D. M.; Surdu, V. A.; Ficai, A.; Ficai, D.; Grumezescu, A. M.; Andronescu, E. Green Synthesis of Metal and Metal Oxide Nanoparticles: A Review of the Principles and Biomedical Applications. *Int. J. Mol. Sci.* **2023**, *24* (20). https://doi.org/10.3390/ijms242015397.

(62) Vijayaram, S.; Razafindralambo, H.; Sun, Y. Z.; Vasantharaj, S.; Ghafarifarsani, H.; Hoseinifar, S. H.; Raeeszadeh, M. Applications of Green Synthesized Metal Nanoparticles — a Review. *Biol. Trace Elem. Res.* **2024**, *202* (1), 360–386. https://doi.org/10.1007/s12011-023-03645-9.

(63) Yarahmadi, A.; Dousti, B.; Karami-Khorramabadi, M.; Afkhami, H. Materials Based on Biodegradable Polymers Chitosan/Gelatin: A Review of Potential Applications. *Front. Bioeng. Biotechnol.* **2024**, *12* (August), 1–22. https://doi.org/10.3389/fbioe.2024.1397668.

(64) Irastorza, A.; Zarandona, I.; Andonegi, M.; Guerrero, P.; de la Caba, K. The Versatility of Collagen and Chitosan: From Food to Biomedical Applications. *Food Hydrocoll.* **2021**, *116*, 106633. https://doi.org/10.1016/j.foodhyd.2021.106633.

(65) Aranaz, I.; Alcántara, A. R.; Civera, M. C.; Arias, C.; Elorza, B.; Caballero, A. H.; Acosta, N. Chitosan: An Overview of Its Properties and Applications. *Polymers (Basel).* **2021**, *13* (19). https://doi.org/10.3390/polym13193256.

(66) Edo, G. I.; Ndudi, W.; Ali, A. B. M.; Yousif, E.; Zainulabdeen, K.; Akpoghelie, P. O.; Isoje, E. F.; Igbuku, U. A.; Opiti, R. A.; Athan Essaghah, A. E.; Ahmed, D. S.; Umar, H.; Alamiery, A. A. Chitosan: An Overview of Its Properties, Solubility, Functional Technologies, Food and Health Applications. *Carbohydr. Res.* **2025**, *550* (November

2024), 109409. https://doi.org/10.1016/j.carres.2025.109409.

(67) Wulandari, D.; Triatmojo, S.; Erwanto, Y.; Pranoto, Y. Physicochemical Properties and Amino Acid and Functional Group Profiles of Gelatin Extracted from Bovine Split Hide Cured by Acid. *Pakistan J. Nutr.* **2016**, *15* (7), 655–661. https://doi.org/10.3923/pjn.2016.655.661.

(68) She, J.; Liu, J.; Mu, Y.; Lv, S.; Tong, J.; Liu, L.; He, T.; Wang, J.; Wei, D. Recent Advances in Collagen-Based Hydrogels: Materials, Preparation and Applications. *React. Funct. Polym.* **2025**, *207* (November 2024), 106136. https://doi.org/10.1016/j.reactfunctpolym.2024.106136.

(69) Jiménez-Gómez, C. P.; Cecilia, J. A. Chitosan: A Natural Biopolymer with a Wide and Varied Range of Applications. *Molecules* **2020**, *25* (17). https://doi.org/10.3390/molecules25173981.

(70) Parvathy, P. A.; De, S.; Singh, M.; Manik, G.; Sahoo, S. K. Functional Self-Healing Aldehyde-Derived Nanoparticle-Crosslinked Gelatin/PNIPAm-Based Adhesive Gels. *RSC Appl. Polym.* **2025**, 662–674. https://doi.org/10.1039/d5lp00038f.

(71) Terao, K.; Otsubo, M.; Abe, M. Complex Formation of Silica Nanoparticles with Collagen: Effects of the Conformation of Collagen. *Langmuir* **2020**, *36* (47), 14425–14431. https://doi.org/10.1021/acs.langmuir.0c02867.

(72) Guillén-Carvajal, K.; Valdez-Salas, B.; Beltrán-Partida, E.; Salomón-Carlos, J.; Cheng, N. Chitosan, Gelatin, and Collagen Hydrogels for Bone Regeneration. *Polymers (Basel).* **2023**, *15* (13). https://doi.org/10.3390/polym15132762.

(73) El-Seedi, H. R.; Said, N. S.; Yosri, N.; Hawash, H. B.; El-Sherif, D. M.; Abouzid, M.; Abdel-Daim, M. M.; Yaseen, M.; Omar, H.; Shou, Q.; Attia, N. F.; Zou, X.; Guo, Z.; Khalifa, S. A. M. Gelatin Nanofibers: Recent Insights in Synthesis, Bio-Medical Applications and Limitations. *Heliyon* **2023**, *9* (5), e16228. https://doi.org/10.1016/j.heliyon.2023.e16228.

(74) Momtaz, M.; Momtaz, E.; Mehrgardi, M. A.; Momtaz, F.; Narimani, T.; Poursina, F. Preparation and Characterization of Gelatin/Chitosan Nanocomposite Reinforced by NiO Nanoparticles as an Active Food Packaging. *Sci. Rep.* **2024**, *14* (1), 1–11. https://doi.org/10.1038/s41598-023-50260-8.

(75) Mathew, S. A.; Arumainathan, S. Crosslinked Chitosan-Gelatin Biocompatible Nanocomposite as a Neuro Drug Carrier. *ACS Omega* **2022**, *7* (22), 18732–18744. https://doi.org/10.1021/acsomega.2c01443.

(76) Yigit, O. Thermal, Chemical, and Structural Investigation of the Usability of Cs/NHAp-ZnO/Glutaraldehyde Polymer Matrix Composite in Potential Biomaterial Applications. *Arab. J. Chem.* **2023**, *16* (7), 104838. https://doi.org/10.1016/j.arabjc.2023.104838.

(77) Wan, J.; Wang, J. H.; Liu, T.; Xie, Z.; Yu, X. F.; Li, W. Surface Chemistry but Not Aspect Ratio Mediates the Biological Toxicity of Gold Nanorods in Vitro and in Vivo. *Sci. Rep.* **2015**, *5* (November 2014), 1–16. https://doi.org/10.1038/srep11398.

(78) Fahy, K. M.; Eiken, M. K.; Baumgartner, K. V.; Leung, K. Q.; Anderson, S. E.; Berggren, E.; Bouzos, E.; Schmitt, L. R.; Asuri, P.; Wheeler, K. E. Silver Nanoparticle Surface Chemistry Determines Interactions with Human Serum Albumin and Cytotoxic Responses in Human Liver Cells. *ACS Omega* **2023**, *8* (3), 3310–3318. https://doi.org/10.1021/acsomega.2c06882.

(79) Lo, S.; Fauzi, M. B. Current Update of Collagen Nanomaterials—Fabrication, Characterisation and Its Applications: A Review. *Pharmaceutics* **2021**, *13* (3), 1–18. https://doi.org/10.3390/pharmaceutics13030316.

(80) Zaman, M.; Ahmad, E.; Qadeer, A.; Rabbani, G.; Khan, R. H. Nanoparticles in Relation to Peptide and Protein Aggregation. *Int. J. Nanomedicine* **2014**, *9* (1), 899–912. https://doi.org/10.2147/IJN.S54171.

(81) Cahn, D.; Stern, A.; Buckenmeyer, M.; Wolf, M.; Duncan, G. A. Extracellular Matrix Limits Nanoparticle Diffusion and Cellular Uptake in a Tissue-Specific Manner. *ACS Nano* **2024**. https://doi.org/10.1021/acsnano.4c10381.

(82) Mülhopt, S.; Diabaté, S.; Dilger, M.; Adelhelm, C.; Anderlohr, C.; Bergfeldt, T.; de la Torre, J. G.; Jiang, Y.; Valsami-Jones, E.; Langevin, D.; Lynch, I.; Mahon, E.; Nelissen, I.; Piella, J.; Puntes, V.; Ray, S.; Schneider, R.; Wilkins, T.; Weiss, C.; Paur, H. R. Characterization of Nanoparticle Batch-to-Batch Variability. *Nanomaterials* **2018**, *8* (5). https://doi.org/10.3390/nano8050311.

(83) Dong, C.; Malliaras, G. G. Recent Advances in Stimuli-Responsive Materials and Soft Robotic Actuators for Bioelectronic Medicine. *Adv. Mater.* **2025**, *2417325*. https://doi.org/10.1002/adma.202417325.

Chapter 1

Size-Selective Synthesis of Gold Nanoparticles Stabilized on Chitosan via the Matrix-Transfer Technique

Nazgul Assan, Yuta Uetake, Hidehiro Sakurai

Journal of Nanoparticle Research **2023**, *25*, 50.

1-1. Introduction

Given the recent interest in sustainable development, the use of naturally abundant resources has become prevalent across various scientific and industrial fields. Metal nanoparticles (NPs) stabilized by biomacromolecules, such as cellulose and chitosan, have garnered significant attention due to environmental considerations and their unique catalytic properties, which are not found in conventional solid supports and synthetic polymers.[1-4] This research has focused on the "matrix effect" of biomacromolecule-based polymer matrices[5-10] in the context of catalysis for fine chemical synthesis.[11-16] Chitosan, in particular, has been widely used as a matrix for metal NPs because of its structural stability, resistance to organic solvents, presence of hydroxyl and amino functional groups (Figure 7A), and inherent chirality.[17-22]

In 2012, H. Sakurai et al. reported that chitosan-stabilized gold (Au) NPs demonstrated exceptional catalytic activity for the homocoupling of phenylboronic acid.[23] It was previously known that this reaction[24] is effectively catalyzed by poly-*N*-vinylpyrrolidone (PVP)-stabilized Au NPs under basic aqueous conditions, which enhance the transmetalation process. However, this method also led to the oxygenation of phenylboronic acid, producing phenol as a byproduct.[25] In contrast, the Au reaction proceeded under neutral conditions, yielding biphenyl as the sole product. This selectivity is attributed to the generation of borate near the Au NP, which prevents unwanted oxidation pathways (Figure 7B).[23]

The size effect of nanoparticles (NPs) is another crucial factor impacting catalytic activity.[26-28] Multiple methods for the size-selective preparation of single metal and bimetallic alloy NPs using PVP as a matrix were implemented. These methods yield size-specific Au and AuPd particles with sizes ranging from 1 to 10 nm.[29-31]

The above methods led to the earlier discovery, in the author's affiliated laboratory, of a significant size- and matrix-dependent effect influenced by nanoparticle size and PVP chain length.[32] The size-selectively prepared Au also serves as a precursor for heterogeneous catalysts through the trans-deposition method (Scheme 1A). In fact, hydroxyapatite (HAP)[33,34] and fibrillated citric acid-modified cellulose (F-CAC)[35] supported Au NPs were successfully synthesized, maintaining the original particle size of the Au.

A. Preparation of Au:chit NPs by chemical reduction method[22]:

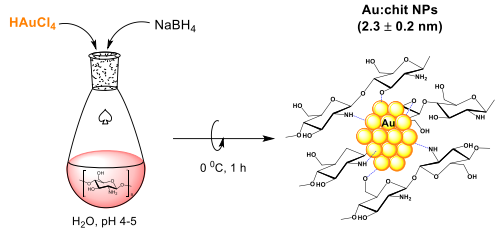

B. Application of Au:chit NPs for homocoupling reaction of Ph-B(OH)$_2$[23]:

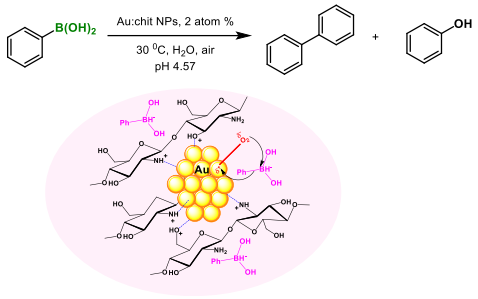

Figure 7 Previous work: Au:chit (A) and its application in homocoupling reaction (B)

This method offers the potential for precisely controlling the size of supported Au NPs, provided the optimal conditions for the trans-deposition method are identified. The author's investigation of the Au catalyst prompted interest in size-dependent phenomena similar to those previously observed for Au. Previous reports indicated that Au was produced through chemical reduction with $NaBH_4$, resulting in particles sized at 2.8 nm. After several unsuccessful attempts to create a series of Au with varying sizes using methods such as chemical reduction, size-mediated growth, and trans-deposition, the author decided to develop a new approach. The core of this technique lies in dispersing the two matrices, PVP and chit, into separate immiscible solvents. This allows the Au NPs to move from one phase to another while maintaining their particle size through the phase transfer. Because the process occurs under biphasic homogeneous conditions, it has been designated the "matrix-transfer" method to reflect this characteristic (Scheme 1B). Here, the author provides a detailed report on the matrix-transfer method.

Scheme 1 Comparison of trans-deposition and matrix-transfer approaches for size controlled Au NP immobilization

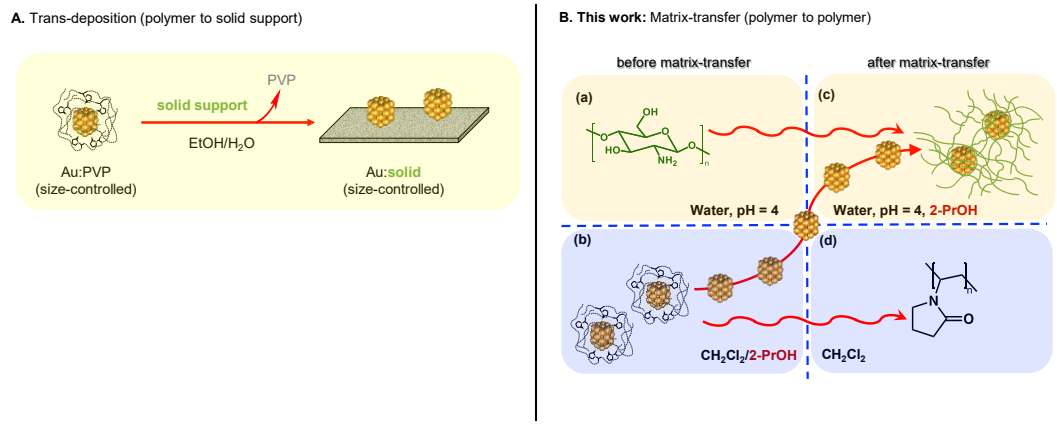

1-2. Experimental section

1-2-1. Preparation of Au:PVP NPs (1.2 ± 0.4 nm) by simple reduction method[29]

In a test tube containing $HAuCl_4$ (0.025 mmol) and PVP(K-15) (2.5 mmol) in water (43 mL) was added an aqueous solution of $NaBH_4$ (0.25 mmol) at 0 °C to give a brown hydrosol. After stirring for 1 h at the same temperature, the hydrosol was concentrated by centrifugation (4500 rpm) using a molecular weight cut-off membrane (MWCO 3 kDa) at 5 °C and washed with water (3 × 20 mL). The residue was freeze-dried for 2 days.

1-2-2. Preparation of Au:PVP NPs (2.6 ± 0.4 nm) by slow reduction method [30]

To a solution containing PVP(K-15) (2.5 mmol) and $HAuCl_4$ (0.025 mmol) in water (40 mL) was added an aqueous solution of Na_2SO_3 (0.075 mmol, 5 mL) at 27 °C under vigorously stirring (1700 rpm). After that, to this was added an aqueous solution of $NaBH_4$ (0.25 mmol, 5 mL) immediately to give a brown hydrosol. The mixture was stirred at 1700 rpm at 27 °C for 3 h. The hydrosol was concentrated by centrifugation (4500 rpm) using a molecular weight cut-off membrane (MWCO 3 kDa) at 5 °C and washed with water (3 × 20 mL). The residue was freeze-dried for 2 days.

1-2-3. Preparation of Au:PVP NPs (4.6 ± 1.4 nm) by Seed-Mediated Growth Method

PVP(K-15) (2.09 mmol) and Au:PVP(K-15, 1.2 nm) (0.00415 mmol) were mixed in water (15 mL) at 27 °C until total dissolution. This mixture was degassed with freeze-pump-thaw 2 times. To a frozen mixture was added an aqueous solution of $HAuCl_4$ (0.02085 mmol) and then evacuated under reduced pressure. Meanwhile, an aqueous solution of Na_2SO_3 (90 mmol/L, 5 mL) was degassed by freeze-pump-thaw 3 times. To the Au:PVP solution, the aqueous solution of Na_2SO_3 (0.0625 mmol) was added as soon as the frozen solution melt via syringe to give red hydrosol. This mixture was stirred at 1300 rpm for 3 h under 27 °C. The hydrosol was concentrated by centrifugation (4000

rpm) using a molecular weight cut-off membrane (MWCO 3 kDa) at 27 °C and washed with water (3 × 20 mL). The residue was freeze-dried for 2 days.

1-2-4. Preparation of Au:PVP NPs (6.2 ± 1.6 nm) by Seed-Mediated Growth Method

PVP(K-15) (2.39 mmol) and Au:PVP(K-15, 1.2 nm) (0.00115 mmol) were mixed in water (15 mL) at 27 °C until total dissolution. This mixture was degassed with freeze-pump-thaw 2 times. To a frozen mixture was added an aqueous solution of $HAuCl_4$ (0.0239 mmol) and then evacuated under reduced pressure. Meanwhile, an aqueous solution of Na_2SO_3 (90 mmol/L, 5 mL) was degassed by freeze-pump-thaw 3 times. To the Au:PVP solution, the aqueous solution of Na_2SO_3 (0.072 mmol) was added as soon as the frozen solution melt via syringe to give red hydrosol. This mixture was stirred at 1300 rpm for 3 h under 27 °C. The hydrosol was concentrated by centrifugation (4000 rpm) using a molecular weight cut-off membrane (MWCO 3 kDa) at 27 °C and washed with water (3 × 20 mL). The residue was freeze-dried for 2 days.

1-2-5. Preparation of Au:chit by matrix-transfer method

In a round-bottom flask, chitosan (150 mg) was dissolved in acetic acid (0.5 mL) and Milli-Q grade water (25 mL) and stirred slowly overnight. The solution was cooled to 0 °C with an ice bath. In a test tube (diameter = 30 mm), CH_2Cl_2:2-PrOH (6.5 mL:19.5 mL) by stirring for 15 min under 0 °C. To this was added Au:PVP (200 mg) and stirred for another 15 min under the same temperature. Next, the Au:PVP solution was rapidly added to the chitosan solution at 0 °C under vigorous stirring under a nitrogen atmosphere. After stirring for 2 h. The solution was transferred to a 50 mL centrifuge tube and was placed in the centrifuge machine (Kubota, 7780 II at 5 °C) for 1 h at 4000 rpm. After centrifuge, the solution was separated by a funnel. The pH of the aqueous phase was adjusted to pH > 7 by 5 mol/L aqueous NaOH solution to form a gel film. The film was washed with water (ca. 20 mL × 15) and centrifuged every 15 min until the pH of this solution reached pH < 5. The film was picked up by spatula from the bottom of the centrifuge test tube and placed in a freeze-dried vial and freeze-dried for 2 days to afford Au:chit.

1-2-6. Procedure for homocoupling reaction

Au:chit was dissolved in acetate buffer (pH 4.57, 10 mL) for 3-5 h under 0 °C prior to use. Phenylboronic acid (30.5mg, 0.25 mmol) and acetate buffer (pH 4.57, 5 mL) were placed in a test tube (diameter = 30 mm). A hydrosol of Au:chit (0.5 mmol/L, 10 mL, 2

atom% in acetate buffer) was added, and the mixture was stirred (1300 rpm) at 300 K for 3 h. To the reaction mixture was added ethyl acetate, and the products were extracted with ethyl acetate (4 × 15 mL). The combined organic extract was dried over Na_2SO_4. After filtration, the filtrate was concentrated under reduced pressure. Then to this was added 1,1,2,2-tetrachloroethane (20 μL, 0.1908 mmol) as an internal standard. The mixture was diluted with $CDCl_3$, and ^1H NMR measurements were performed to determine the yields.

1-3. Results and Discussions

The challenge toward developing the matrix transfer commenced with the attempt to apply the trans-deposition method, previously established in the laboratory where the author conducted this research, using size-selectively prepared Au:PVP(K-15, 1.5 ± 0.5 nm) as a transient Au NPs source.[33] In the earlier investigations for size-selective preparation of Au:chit, the trans-deposition from Au:PVP(K-15) was applied to the solid chitosan using an insoluble solvent system. However, all the attempts have resulted in the aggregation of Au NPs and poor deposition efficiency. In addition, the challenge of the matrix-to-matrix transfer is that the calcination process is not applicable to remove the PVP, contrary to the case of solid supports. The author realized that the main difficulty for consideration was supporting metal NPs stabilizing matrix itself (Scheme 1A). According to proposed hypothesis, the metal needs to be transferred from one homogenous media to another homogenous media, which is quite complex based on the author's observations. Another nuisance was the compatible solvent of choice for all media during the matrix-transfer process. This solvent should assist the release of metal NPs from the PVP matrix and facilitate their further transfer to the chitosan matrix. Finally, the author hypothesized that kinetic conditions must also be essential for a proper matrix transfer. To overcome all these difficulties, various attempts were performed, and finally, the biphasic solvent system was found to be suitable for the size-selectivity of Au NPs. A biphasic solvent system was utilized with 2% aqueous acetic acid solution (aqueous phase) and CH_2Cl_2/2-PrOH = 1:1 (organic phase). Chitosan was initially dissolved in the aqueous phase (Scheme 1B, a) and Au:PVP(K-15) in the organic phase (Scheme 1B, b). During stirring at 27 °C, the Au NP was transferred from PVP to chitosan at the interface of the solvents (Scheme 1B, c), and most of the PVP remained in the aqueous phase (Scheme 1B, d). After purification using the dialysis membrane, Au:chit with a particle size of 3.3 ± 1.0 nm was obtained (Table 1, entry 1). Then, the conditions

were optimized. Although lowering the temperature did not improve the particle size of Au:chit (entries 2-3), that the ratio of CH_2Cl_2 and 2-PrOH substantially affected the particle size. Whereas the excessive use of dichloromethane (CH_2Cl_2/2-PrOH = 3:1) showed almost no effect, the excessive use of 2-propanol (CH_2Cl_2/2-PrOH = 1:3) significantly suppressed the agglomeration of Au NPs to afford Au:chit with the particle size of 1.7 ± 1.0 nm (entry 6). As in entries 1-3, the lower temperature did not affect the particle size (entry 7).

Table 1 Effect of solvent and temperature on Au NP size

Entry	CH_2Cl_2/2-PrOH	temp. (°C)	Particle size (nm)
1	1:1	27	3.3 ±1.0
2	1:1	0	3.3 ± 1.0
3	1:1	–15	3.1 ± 1.0
4	3:1	0	2.9 ± 1.0
5	3:1	–15	2.6 ± 0.7
6	1:3	0	1.7 ± 0.5
7	1:3	–15	1.7 ± 0.5

* Au:PVP(K-15, 1.5 ± 0.5 nm) was used. Aqueous phase: 2 % aqueous acetic acid

The above results indicate that 2-PrOH displays vital assistance during the matrix-transfer method. Once in contact with Au:PVP NPs, it lessens interaction between metal NPs and polymer matrix (Scheme 1B, b). Binding between Au surface and carbonyl (C=O) group of PVP unit is entirely loosened due to the absolute solubility of Au:PVP NPs in CH_2Cl_2/2-PrOH media. Later, upon constant accelerated stirring, it was found that 2-PrOH acts as both metal and phase transfer agent, which accommodates safe migration of Au NPs from PVP in low polar media to polar media (Scheme 1B, c). This was based on the notable differences in polarity indexes of CH_2Cl_2 (3.1), 2-PrOH (3.9), and water (10.2), [36] as well as on the high Hansen solubility parameter of 2-PrOH to PVP. [37]

With the optimized conditions for matrix transfer from PVP to chitosan in hand, the matrix transfer method using other sizes of Au:PVP (Table 2) were performed.

Table 2 Comparison of Au NP sizes before and after matrix-transfer from PVP to chitosan

Entry	NP size of Au:PVP (nm)	NP size of Au:chit (nm)
1	1.2 ± 0.4	1.4 ± 0.6
2	2.4 ± 0.7	3.4 ± 1.0
3	4.6 ± 1.4	5.3 ± 1.4

4	6.2 ± 1.6	6.5 ± 1.6

From Au:PVPs with a mean size of 1.2 nm, 2.4 nm, 4.6 nm, and 6.2 nm, the author succeeded in preparing Au:chits having sizes of 1.4 nm, 3.4 nm, 5.3 nm, and 6.5 nm, respectively. TEM results confirm that various sizes of Au NPs could be stabilized onto chitosan while maintaining initial metal cores within the bounds of error margin (Figure 8).

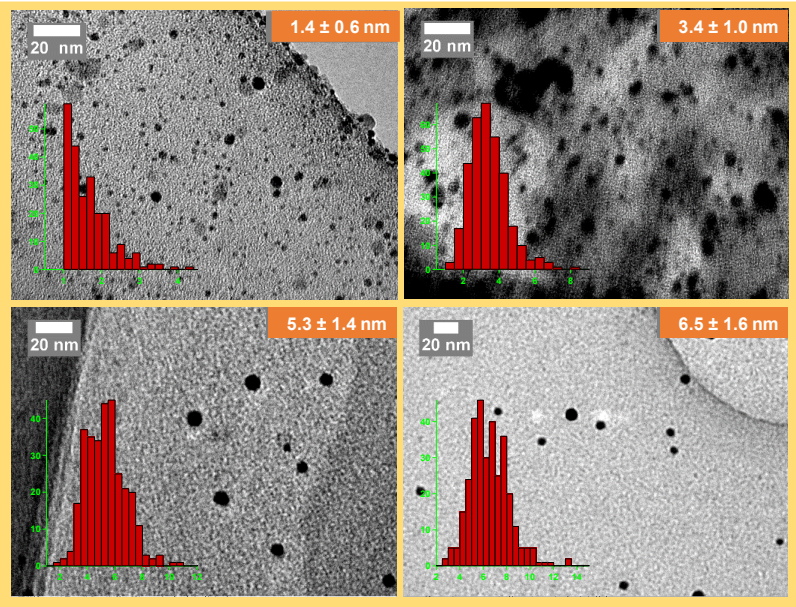

Figure 8 TEM images and corresponding size distribution histograms of Au NPs The average particle sizes (± standard deviation) are indicated in each image: (top left) 1.4 ± 0.6 nm, (top right) 3.4 ± 1.0 nm, (bottom left) 5.3 ± 1.4 nm, and (bottom right) 6.5 ± 1.5 nm. Scale bars represent 20 nm.

Thus, the matrix-transfer effect successfully produced size controlled Au:chits of 1.4-6.5 nm. The surface morphology of the thus-produced Au:chits was observed via SEM measurements (Figure 9).

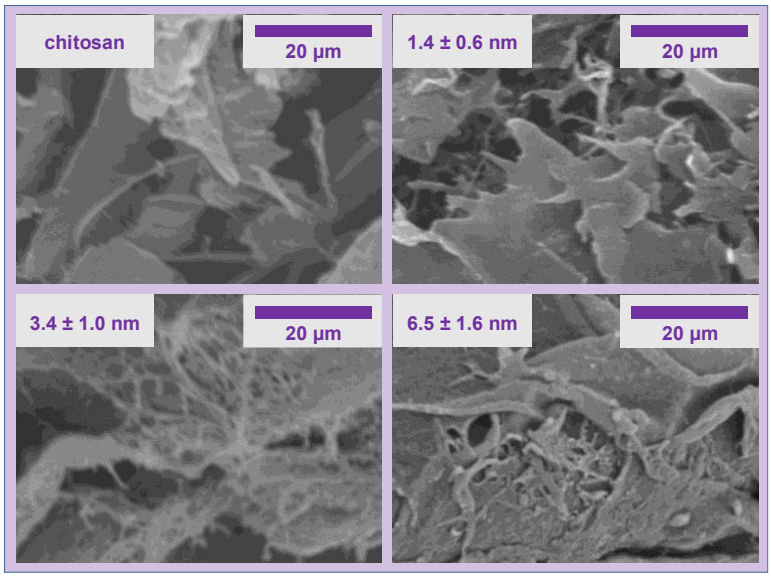

Figure 9 SEM images of chit and Au NPs. (Top left) Pure chitosan matrix; (top right to bottom right) AuNPs with increasing particle sizes: 1.4 ± 0.6 nm, 3.4 ± 1.0 nm, and 6.5 ± 1.6 nm. Scale bars represent 20 um.

Chitosan-stabilized Au NPs acquire similar non-even and fibrous-like textures as pristine chitosan, as PVP is known to have a ball shape structure, which did not occur in the surfaces of newly prepared Au:chits. The removal of PVP was confirmed by infrared (IR) spectroscopy analysis that the absorption band was found in 1260 cm^{-1} and that corresponding to the C=O stretching vibration in the carbonyl group of PVP (1653 cm^{-1}) disappeared (Figure 10).

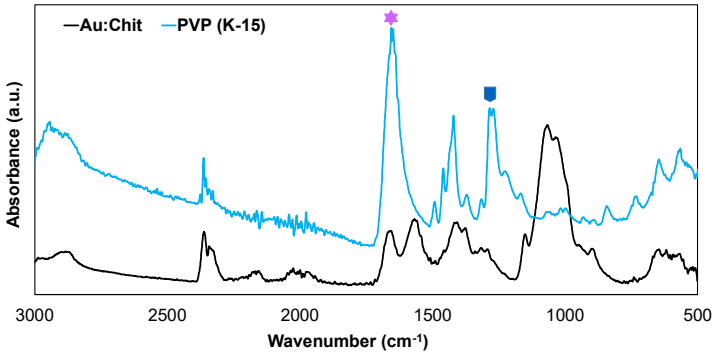

Figure 10 FTIR spectra of Au NPs stabilized with chitosan (Au:Chit, black) and polyvinylpyrrolidone (PVP K-15, blue). The distinct peaks marked with a star (≈1650 cm^{-1}) and a square (≈1290 cm^{-1}) correspond to the C=O stretching of the pyrrolidone ring and C-N stretching, respectively, indicating the presence of PVP.

Later, the size-dependency of the thus-prepared Au:chits in the catalytic reaction was investigated (Scheme 2).

Scheme 2 Homocoupling reaction of phenylboronic acid to form biphenyl alcohol catalyzed by Au:chit NPs

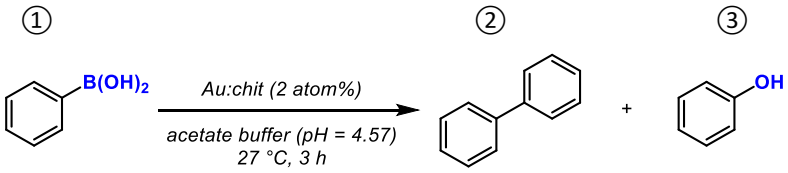

The homocoupling reaction of phenylboronic acid (**1**) was chosen as a benchmark reaction; the catalytic activity was evaluated from the yield after an initial 3 h to minimize the influence from the aggregation of Au NPs, which is essentially unavoidable in this homocoupling reaction.[24, 38] Regarding the conversion, the 2.3 nm-sized NPs exhibited the best activity, superior to 1.4 nm-sized NPs, indicating that this catalytic system's optimum size might exist (Figure 11a). Alternatively, regarding the reaction selectivity, the formation of phenol (**3**) could not be suppressed in most cases, which was nearly achieved in the previous Au:chit catalyst prepared via the batch method.[23] The selectivity ratio of **2**:**3** was decreased with increasing the size of NPs, and the 1.4 nm-sized NPs showed the best product selectivity, better than the batch catalyst (Figure 11b). One possible reason to explain the size-dependent selectivity involves the intrinsic nature of the gold NPs: smaller particles intrinsically possess higher reaction selectivity. Nevertheless, the most probable reason might be that the larger particles have a more exposed surface, which is not effectively covered with the chitosan matrix, losing the significant matrix effect. Upon acquiring this catalytic data, the author has realized once again that, most probably, the NPs will agglomerate within a longer time, making it difficult for further recyclability studies.

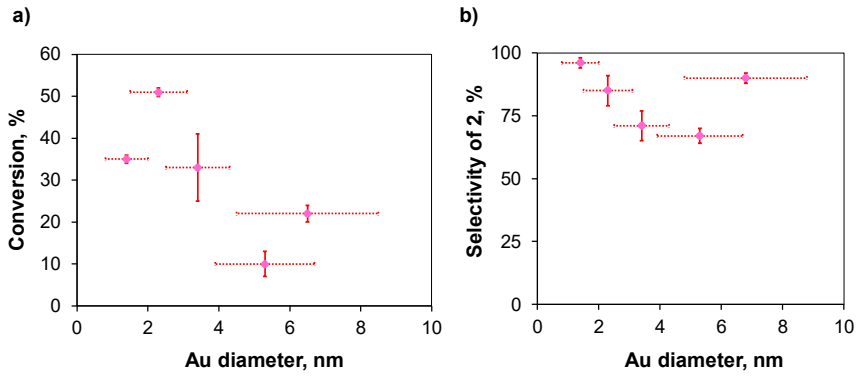

Figure 11 Influence of Au NP size on catalytic performance in the homocoupling of phenylboronic acid. (a) Conversion (%) and (b) selectivity (%) toward the biphenyl product (2) as a function of Au NP diameter. Error bars represent standard deviations in particle size and reaction outcomes.

1-4. Conclusions

In conclusion, using the matrix-transfer method, the author successfully prepared Au:chit in several sizes ranging from 1.7 nm to 6.5 nm. The secret to success was the addition of 2-PrOH to facilitate the transfer process without severe aggregation. This size selective preparation of Au:chits enabled the novel investigation of the size dependency of the Au:chit catalyzed reaction. Two size dependencies were observed in the reaction of phenylboronic acid: the volcano type size dependency with a 2.3 nm-sized catalyst observed at the top in the catalytic activity and the reaction selectivity between the homocoupling reaction and the oxygenation, in which the smaller sized catalyst exhibited higher homocoupling selectivity. This suggests that the chitosan matrix effect more strongly affects the smaller particles. However, why the 6.5 nm sized catalysts possess a higher activity and selectivity than the 5.3 nm sized catalysts are still unclear; further investigation is needed. In addition, furthermore, the author is also interested in the generality of the novel matrix transfer method.

1-5. References

(1) Jin, R.; Zeng, C.; Zhou, M.; Chen, Y. Atomically Precise Colloidal Metal Nanoclusters and Nanoparticles: Fundamentals and Opportunities. Chem. Rev. 2016, 116 (18), 10346–10413. https://doi.org/10.1021/acs.chemrev.5b00703.

(2) Kang, H.; Buchman, J. T.; Rodriguez, R. S.; Ring, H. L.; He, J.; Bantz, K. C.; Haynes, C. L. Stabilization of Silver and Gold Nanoparticles: Preservation and Improvement of Plasmonic Functionalities. Chem. Rev. 2019, 119 (1), 664–699. https://doi.org/10.1021/acs.chemrev.8b00341.

(3) Lee, J. W.; Choi, S. R.; Heo, J. H. Simultaneous Stabilization and Functionalization of Gold Nanoparticles via Biomolecule Conjugation: Progress and Perspectives. ACS Appl. Mater. Interfaces 2021. https://doi.org/10.1021/acsami.1c10436.

(4) Shreyash, N.; Bajpai, S.; Khan, M. A.; Vijay, Y.; Tiwary, S. K.; Sonker, M. Green Synthesis of Nanoparticles and Their Biomedical Applications: A Review. ACS Appl. Nano Mater. 2021, 4 (11), 11428–11457. https://doi.org/10.1021/acsanm.1c02946.

(5) Uehara, N. Polymer-Functionalized Gold Nanoparticles as Versatile Sensing Materials. Anal. Sci. 2010, 26 (12), 1219–1228. https://doi.org/10.2116/analsci.26.1219.

(6) Ha, M.; Kim, J. H.; You, M.; Li, Q.; Fan, C.; Nam, J. M. Multicomponent Plasmonic Nanoparticles: From Heterostructured Nanoparticles to Colloidal Composite Nanostructures. Chem. Rev. 2019, 119 (24), 12208–12278. https://doi.org/10.1021/acs.chemrev.9b00234.

(7) Barui, A. K.; Nethi, S. K.; Haque, S.; Basuthakur, P.; Patra, C. R. Recent Development of Metal Nanoparticles for Angiogenesis Study and Their Therapeutic Applications. ACS Appl. Bio Mater. 2019, 2 (12), 5492–5511. https://doi.org/10.1021/acsabm.9b00587.

(8) Gao, Y.; Zhou, Y.; Chandrawati, R. Metal and Metal Oxide Nanoparticles to Enhance the Performance of Enzyme-Linked Immunosorbent Assay (ELISA). ACS Appl. Nano Mater. 2020, 3 (1), 1–21. https://doi.org/10.1021/acsanm.9b02003.

(9) Zeiri, O. Metallic-Nanoparticle-Based Sensing: Utilization of Mixed-Ligand Monolayers. ACS Sensors 2020, 5 (12), 3806–3820. https://doi.org/10.1021/acssensors.0c02124.

(10) Nilghaz, A.; Mousavi, S. M.; Tian, J.; Cao, R.; Guijt, R. M.; Wang, X. Noble-Metal Nanoparticle-Based Colorimetric Diagnostic Assays for Point-of-Need Applications. ACS Appl. Nano Mater. 2021, 4 (12), 12808–12824. https://doi.org/10.1021/acsanm.1c01545.

(11) Wang, Y.; Wei, G.; Wen, F.; Zhang, X.; Zhang, W.; Shi, L. Synthesis of Gold Nanoparticles Stabilized with Poly(N-Isopropylacrylamide)-Co-Poly(4-Vinyl Pyridine) Colloid and Their Application in Responsive Catalysis. J. Mol. Catal. A Chem. 2008, 280 (1–2), 1–6. https://doi.org/10.1016/j.molcata.2007.10.014.

(12) Rahme, K.; Nolan, M. T.; Doody, T.; McGlacken, G. P.; Morris, M. A.; O'Driscoll, C.; Holmes, J. D. Highly Stable PEGylated Gold Nanoparticles in Water: Applications in Biology and Catalysis. RSC Adv. 2013, 3 (43), 21016–21024. https://doi.org/10.1039/c3ra41873a.

(13) Yao, Y.; Xue, M.; Zhang, Z.; Zhang, M.; Wang, Y.; Huang, F. Gold Nanoparticles Stabilized by an Amphiphilic Pillar[5]Arene: Preparation, Self-Assembly into Composite Microtubes in Water and Application in Green Catalysis. Chem. Sci. 2013, 4 (9), 3667–3672. https://doi.org/10.1039/c3sc51547h.

(14) Ferry, A.; Schaepe, K.; Tegeder, P.; Richter, C.; Chepiga, K. M.; Ravoo, B. J.; Glorius, F. Negatively Charged N-Heterocyclic Carbene-Stabilized Pd and Au Nanoparticles and Efficient Catalysis in Water. ACS Catal. 2015, 5 (9), 5414–5420. https://doi.org/10.1021/acscatal.5b01160.

(15) Li, N.; Liu, X. Synthesis of Dendrimer-Stabilized Au Nanoparticles and Their Application in the Generation of Hydroxyl Radicals. ChemistrySelect 2019, 4 (34), 9897–9900. https://doi.org/10.1002/slct.201902195.

(16) Heddle, J. G. Gold Nanoparticle-Biological Molecule Interactions and Catalysis.

Catalysts 2013, 3 (3), 683–708. https://doi.org/10.3390/catal3030683.
(17) Wei, D.; Ye, Y.; Jia, X.; Yuan, C.; Qian, W. Chitosan as an Active Support for Assembly of Metal Nanoparticles and Application of the Resultant Bioconjugates in Catalysis. Carbohydr. Res. 2010, 345 (1), 74–81. https://doi.org/10.1016/j.carres.2009.10.008.
(18) Kustov, L. M.; Finashina, E. D.; Shuvalova, E. V.; Tkachenko, O. P.; Kirichenko, O. A. Pd-Fe Nanoparticles Stabilized by Chitosan Derivatives for Perchloroethene Dechlorination. Environ. Int. 2011, 37 (6), 1044–1052. https://doi.org/10.1016/j.envint.2011.05.003.
(19) Cotugno, P.; Casiello, M.; Nacci, A.; Mastrorilli, P.; Dell'Anna, M. M.; Monopoli, A. Suzuki Coupling of Iodo and Bromoarenes Catalyzed by Chitosan-Supported Pd-Nanoparticles in Ionic Liquids. J. Organomet. Chem. 2014, 752, 1–5. https://doi.org/10.1016/j.jorganchem.2013.11.033.
(20) Tan, W. L.; Abu Bakar, N. H. H.; Abu Bakar, M. Catalytic Reduction of P-Nitrophenol Using Chitosan Stabilized Copper Nanoparticles. Catal. Letters 2015, 145 (8), 1626–1633. https://doi.org/10.1007/s10562-015-1547-y.
(21) Laghrib, F.; Ajermoun, N.; Bakasse, M.; Lahrich, S.; El Mhammedi, M. A. Synthesis of Silver Nanoparticles Assisted by Chitosan and Its Application to Catalyze the Reduction of 4-Nitroaniline. Int. J. Biol. Macromol. 2019, 135, 752–759. https://doi.org/10.1016/j.ijbiomac.2019.05.209.
(22) Murugadoss, A.; Sakurai, H. Chitosan-Stabilized Gold, Gold-Palladium, and Gold-Platinum Nanoclusters as Efficient Catalysts for Aerobic Oxidation of Alcohols. J. Mol. Catal. A Chem. 2011, 341 (1–2), 1–6. https://doi.org/10.1016/j.molcata.2011.03.019.
(23) Dhital, R. N.; Murugadoss, A.; Sakurai, H. Dual Roles of Polyhydroxy Matrices in the Homocoupling of Arylboronic Acids Catalyzed by Gold Nanoclusters under Acidic Conditions. Chem. - An Asian J. 2012, 7 (1), 55–59. https://doi.org/10.1002/asia.201100478.
(24) Dhital, R. N.; Sakurai, H. Oxidative Coupling of Organoboron Compounds. Asian J. Org. Chem. 2014, 3 (6), 668–684. https://doi.org/10.1002/ajoc.201300283.
(25) Tsunoyama, H.; Sakurai, H.; Ichikuni, N.; Negishi, Y.; Tsukuda, T. Colloidal Gold Nanoparticles as Catalyst for Carbon-Carbon Bond Formation: Application to Aerobic Homocoupling of Phenylboronic Acid in Water. Langmuir 2004, 20 (26), 11293–11296. https://doi.org/10.1021/la0478189.
(26) Ishida, T.; Murayama, T.; Taketoshi, A.; Haruta, M. Importance of Size and Contact Structure of Gold Nanoparticles for the Genesis of Unique Catalytic Processes. Chem. Rev. 2020, 120 (2), 464–525. https://doi.org/10.1021/acs.chemrev.9b00551.
(27) Wang, H.; Lu, J. A Review on Particle Size Effect in Metal-Catalyzed Heterogeneous Reactions. Chinese J. Chem. 2020, 38 (11), 1422–1444. https://doi.org/10.1002/cjoc.202000205.
(28) Axet, M. R.; Philippot, K. Catalysis with Colloidal Ruthenium Nanoparticles. Chem. Rev. 2020, 120 (2), 1085–1145. https://doi.org/10.1021/acs.chemrev.9b00434.
(29) Tsunoyama, H.; Sakurai, H.; Negishi, Y.; Tsukuda, T. Size-Specific Catalytic Activity of Polymer-Stabilized Gold Nanoclusters for Aerobic Alcohol Oxidation in Water. J. Am. Chem. Soc. 2005, 127 (26), 9374–9375. https://doi.org/10.1021/ja052161e.
(30) Tsunoyama, H.; Sakurai, H.; Tsukuda, T. Size Effect on the Catalysis of Gold Clusters Dispersed in Water for Aerobic Oxidation of Alcohol. Chem. Phys. Lett. 2006, 429 (4–6), 528–532. https://doi.org/10.1016/j.cplett.2006.08.066.
(31) Haesuwannakij, S.; Karuehanon, W.; Mishra, V. L.; Kitahara, H.; Sakurai, H.; Kanaoka, S.; Aoshima, S. Size-Controlled Preparation of Gold Nanoclusters Stabilized by High-Viscosity Hydrophilic Polymers Using a Microflow Reactor. Monatshefte fur Chemie 2014, 145 (1), 23–28. https://doi.org/10.1007/s00706-013-1001-z.
(32) Haesuwannakij, S.; Kimura, T.; Furutani, Y.; Okumura, K.; Kokubo, K.; Sakata, T.; Yasuda, H.; Yakiyama, Y.; Sakurai, H. The Impact of the Polymer Chain Length on the Catalytic Activity of Poly(N-Vinyl-2-Pyrrolidone)-Supported Gold Nanoclusters. Sci.

Rep. 2017, 7 (1), 1–8. https://doi.org/10.1038/s41598-017-10165-9.
(33) Haesuwannakij, S.; Poonsawat, T.; Noikham, M.; Somsook, E.; Yakiyama, Y.; Dhital, R. N.; Sakurai, H. Size-Controlled Preparation of Gold Nanoclusters on Hydroxyapatite through Trans-Deposition Method. J. Nanosci. Nanotechnol. 2017, 17 (7), 4649–4657. https://doi.org/10.1166/jnn.2017.13777.
(34) Haesuwannakij, S.; Yakiyama, Y.; Sakurai, H. Partially Fluoride-Substituted Hydroxyapatite as a Suitable Support for the Gold-Catalyzed Homocoupling of Phenylboronic Acid: An Example of Interface Modification. ACS Catal. 2017, 7 (4), 2998–3003. https://doi.org/10.1021/acscatal.6b03524.
(35) Chutimasakul, T.; Uetake, Y.; Tantirungrotechai, J.; Asoh, T. A.; Uyama, H.; Sakurai, H. Size-Controlled Preparation of Gold Nanoparticles Deposited on Surface-Fibrillated Cellulose Obtained by Citric Acid Modification. ACS Omega 2020, 5 (51), 33206–33213. https://doi.org/10.1021/acsomega.0c04894.
(36) De Brauw, C.; Jong, B.; De Mol Van Otterloo, H.; Olden, P.; Barwick, V. J. Strategies for Solvent Selection - A Literature Review. Common Leg. Framew. Tak. Bids Eur. 1997, 1 (6), 293–309. https://doi.org/10.1017/CBO9780511720895.015.
(37) Çaykara, T. Solubility Parameters of Cross-Linked Poly(N-Vinyl-2-Pyrrolidone-Co-Crotonic Acid) Copolymers Prepared by γ-Ray-Induced Polymerization Technique. J. Macromol. Sci. - Pure Appl. Chem. 2004, 41 A (8), 971–979. https://doi.org/10.1081/MA-120039182.
(38) Sakurai, H.; Tsunoyama, H.; Tsukuda, T. Oxidative Homo-Coupling of Potassium Aryltrifluoroborates Catalyzed by Gold Nanocluster under Aerobic Conditions. J. Organomet. Chem. 2007, 692 (1–3), 368–374. https://doi.org/10.1016/j.jorganchem.2006.04.054.

Chapter 2

Exploring the Feasibility of Microchip Laser Ablation Method for the Preparation of Biopolymer-Stabilized Gold Nanoparticles: Case Studies with Gelatin and Collagen

Nazgul Assan, Tomoyuki Suezawa, Yuta Uetake, Yumi Yakiyama, Michiya Matsusaki, Hidehiro Sakurai

Colloids and Interfaces **2025**, *5*, 42.

2-1. Introduction

The integration of metal nanoparticles (NPs) with sub 10 nm dimensions into biopolymeric matrices that are sensitive to chemical and thermal changes presents an ongoing challenge in advanced biomedical applications, including photothermal therapy, targeted drug delivery systems (DDS), bioimaging, and diagnostic platforms.[1-3] Conventionally, the incorporation of such NPs into biopolymer scaffolds is achieved through in situ chemical synthesis techniques, which typically require the presence of external reducing agents, precise pH adjustment, thermal control, and other reaction-specific conditions.[4-6] Despite their widespread use, these chemical methods are often constrained by inherent drawbacks such as NP aggregation and limited dispersion stability. These issues not only compromise the physicochemical properties of the nanocomposites but may also destructively impact the structural integrity and biological functionality of the extracellular matrix.

To overcome the limitations associated with conventional chemical synthesis, pulsed laser ablation in liquid (PLAL) has emerged as a promising physical approach for the direct generation of small-sized metal NPs onto extracellular matrices. This technique offers the production of highly pure NPs in the absence of chemical precursors, surfactants, or stabilizing agents. Moreover, PLAL enables precise modulation of nanoparticle size and morphology, facilitating uniform spatial distribution across the biopolymers.[7-8] Furthermore, the process is fundamentally and environmentally benign; therefore, it allows for straightforward post-synthetic functionalization of NPs.[9–10] The applicability of PLAL has been demonstrated in various systems, including the fabrication of gelatin-stabilized Au NPs, thus confirming its potential for producing biocompatible nanocomposites without the need for chemical reducing agents.[11] Despite these considerable advantages, this technique still has disadvantages. The main limitations include the thermal sensitivity of the biopolymer matrix under localized laser-induced heating and the potential for photochemical alterations to the substrate. Additionally, the method requires a costly investment in laser equipment and maintenance. Finally, the NP yield typically remains lower than that achieved through conventional chemical routes.[12]

Building upon the basic advantages of PLAL, the use of a microchip laser (MCL) has gained increasing attention as a versatile and practical enhancement to traditional

PLAL systems for metal NP synthesis. The MCL is a compact, diode-pumped solid state laser characterized by a short cavity length of approximately 10 mm. This set up allows its integration into standard synthetic laboratories without the necessity for vibration isolation platforms or elaborate optical alignments, therefore offering notable operational simplicity and flexibility.[13] The MCL-PLAL system is further distinguished by three main operational features. Firstly, it functions at a low pulse energy of 1.8 mJ per pulse, which significantly reduces the thermal degradation of chemically and physically delicate compounds. Moreover, it permits the use of volatile solvents and additives. Secondly, the system operates at a low repetition rate of 100 Hz, which mitigates plasma-induced shielding effects even under low-energy conditions. Thirdly, its short pulse duration of 0.9 ns minimizes energy dissipation during laser-material interaction, enhancing ablation efficiency.[13] Together, these parameters contribute to a distinct NP formation mechanism, enabling the controlled synthesis of metal NPs with improved reproducibility and compatibility with sensitive extracellular matrices.

Previous studies have demonstrated that MCL-PLAL conducted in aqueous solutions of poly(N-vinyl-2-pyrrolidone) (PVP) consistently produces Au NPs with an average diameter of approximately 4 nm, regardless of the polymer matrix concentration.[14] This remarkable size uniformity is attributed to the formation of small, short-lived cavitation bubbles during laser ablation, which effectively regulate NP nucleation and growth independently of the surrounding matrix environment. Furthermore, the applicability of the MCL-PLAL technique to various organic solvent systems has already been explored within the lab where the author has worked.[15] More recently, it was reported that the use of aromatic solvents enables fine control over the formation of carbon-coated Au NPs with well-defined core-shell architectures.[16] These results highlight the distinct advantages of MCL-PLAL as a highly adaptable and matrix-tolerant synthesis platform. Mainly, it can generate uniformly sized nanoparticles while minimizing structural damage. MCL-PLAL is a favorable method for the direct fabrication of metal NPs within sensitive biopolymer matrices.

Guided by this rationale, the feasibility of applying MCL-PLAL to gelatin (Gel) shall be explored. It has been reported before that a biopolymer commonly employed in PLAL-mediated Au NP synthesis typically yields particle sizes in the range of 10-15 nm. This investigation aimed to elucidate the specific influence of MCL parameters on

particle formation within gelatin. Additionally, the author extended her study to type I collagen (Col^{I}), a structurally complex and highly stimulus-responsive biopolymer, to evaluate the potential of MCL-PLAL for NP synthesis within even more delicate biomatrices.

2-2. Experimental section

2-2-1. Preparation of different concentrations by wt% Gel solution

Gelatin powder (Product No. 077-03155, FUJIFILM Wako Pure Chemical Corporation) was dissolved in ultrapure water to prepare aqueous solutions with concentrations of 0.02 wt%, 0.05 wt%, 0.1 wt%, 0.2 wt%, and 0.5 wt%.

2-2-2. Extraction of Col^{I} from the mixture of Col^{I} and Col^{III}

1 g of collagen particles (a mixture of Col^{I} and Col^{III}, Nippon Ham) was placed into a 2 L beaker. 500 mL of water was added and stirred at 500-600 rpm in the ice bath. This mixture of collagens was stirred overnight until all the particles were dissolved. To this were added 0.45 mol/L NaCl (13.15 g) and 5 mmol/L tris-HCl buffer solution (394 mg), and the mixture was stirred for 30 min at room temperature. Then, it was transferred to the refrigerator and stored at 4 °C overnight. 1.2 mol/L NaCl (21.92 g) and 5 mmol/L tris-HCl buffer solution (394 mg) were added, and the mixture was slowly stirred for 30 min at room temperature. Once fully dissolved, it was transferred to the refrigerator and stored at 4 °C overnight. The resulting collagen solution was dispensed into conical tubes (50 mL) and centrifuged for 15 min at 10,000 rpm to afford the Col^{III} pellet (the centrifugation process should be repeated when no pellet was formed). After that, the supernatant was collected into a 2 L beaker, and the solution was transferred into dialysis membranes (15 kDa, 15 cm in length). The Col^{I} solution in membranes was immersed in water in a 2 L beaker for 7 days. On the first day, the water was changed every hour. From the second day till the seventh day, the water was changed every 3 h to afford a transparent solution. The thus-dialyzed Col^{I} solution was transferred to 50 mL conical tubes, frozen in liquid nitrogen for 30 min, and freeze-dried for 3 d at the pressure under 25 Pa.

2-2-3. Preparation of 0.2 wt% Col^{I} solution

A total of 50 mg of the extracted type I collagen (Col^{I}) was transferred to a 50 mL conical tube, followed by the addition of 25 mL of precooled phosphate-buffered saline (PBS). The mixture was homogenized for 2-3 minutes to facilitate the breakdown of the collagen sponge into smaller fragments. The tube was then sealed tightly and stored at 4-5 °C for

2-3 days to allow the complete dissolution of collagen into a uniform solution. Subsequently, the resulting dispersion was subjected to centrifugation at 4000 rpm for 5-7 hours at 4-5 °C to eliminate any air bubbles. The resulting supernatant, corresponding to a 0.2 wt% Col^{I} solution, was collected and stored at 4-5 °C until further use.

2-2-4. Procedure for PLAL method using MCL (Figure 12) for Gel/Col^{I}

A gold rod (purity > 99.99%, φ 5 mm × 15 mm) was used as the ablation target. Prior to use, the rod was cleaned by ultrasonication in acetone for 5 minutes, followed by thorough rinsing with deionized water. The gold target was then secured in a custom fabricated holder made of polyether ether ketone (PEEK) and positioned at the center of a 50 mL glass vial (Marueme, dimensions: 30 × 80 mm). To ensure stable placement during the ablation process, zirconia beads were inserted between the holder and the inner wall of the vial, thereby preventing displacement of the gold rod during stirring and enhancing the uniformity of laser exposure.

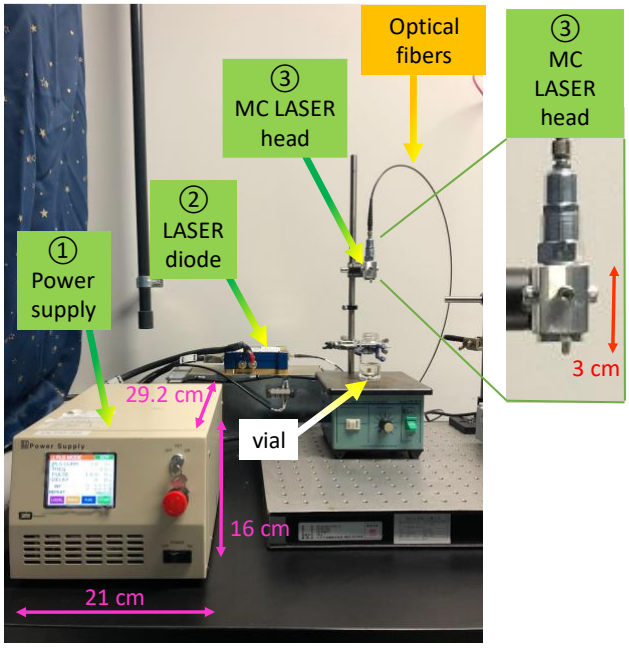

Figure 12 Experimental setup of the microchip laser ablation system (Nd:YAG/Cr^{4+}:YAG) used for nanoparticle synthesis.

A volume of 15 mL of the corresponding biopolymer solution (gelatin or type I collagen dissolved in water or PBS, respectively) was added to the vial. Laser ablation was carried out under ambient conditions in the dark, with continuous stirring at 270 rpm for 1 hour. A microchip laser (MCL) system operating at a wavelength of 1064 nm and based on a monolithic Nd:YAG/Cr^{4+}:YAG ceramic structure was employed for ablation. The laser parameters were configured via the power supply interface, with a driving current of 70

A, a pulse repetition rate of 180 Hz, and a pulse duration of 0.9 ns. Under these operating conditions, an average laser output power of 130-140 mW was achieved, as measured using a Nova II OPHIR Power/Energy Meter. The laser head was positioned at a vertical distance of 14 cm above the gold target surface to ensure optimal focusing.

2-3. Results and Discussions

The primary aim of this study was to synthesize gelatin-stabilized gold nanoparticles (Au NPs) using microchip laser-assisted pulsed laser ablation in liquid (MCL-PLAL), thereby eliminating the need for conventional chemical reducing agents. To this end, a bulk gold rod was subjected to laser ablation in aqueous gelatin solutions of varying concentrations (Figure 13A). Across all tested concentrations, the formation of stable, red-colored colloidal solutions was observed (Figure 13B), indicating successful generation of AuNPs. Previous work by Watari et al. demonstrated that gelatin-stabilized AuNPs synthesized via chemical reduction with sodium ascorbate yielded particles in the 10-15 nm range, with size variation dependent on gelatin concentration.[17] In a separate study, Darroudi et al. employed a high power laser system (360 mJ/pulse, 5 ns pulse width) and reported AuNP sizes ranging from 7-19 nm, with smaller particles obtained upon prolonged ablation.[11] In contrast, the present study employed gelatin concentrations ranging from 0.02 to 0.5 wt%, while maintaining a constant laser irradiation time of 1 hour. As summarized in Table 3, the resulting nanoparticles exhibited uniform diameters in the narrow range of 4.2-4.4 nm, as determined by transmission electron microscopy (TEM), and displayed a consistent spherical morphology (Figure 14). A representative TEM image corresponding to the 0.2 wt% condition is shown in Figure 13-B1.

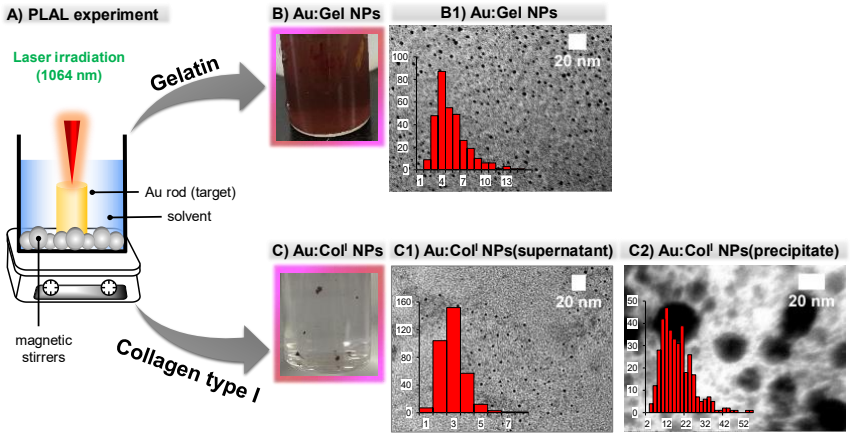

Figure 13 Schematic and results MCL-PLAL for synthesizing gold nanoparticles (AuNPs) in biopolymer matrices. ***(A)*** *Illustration of the PLAL setup using a 1064 nm laser to ablate a gold target in either gelatin or collagen type I solutions with magnetic stirring.* ***(B)*** *Photograph of AuNPs synthesized in gelatin (Gel-Au NPs).* ***(B1)*** *TEM image and corresponding size distribution histogram of Gel-Au NPs.* ***(C)*** *Photograph of AuNPs synthesized in collagen type I (Col-Au NPs), exhibiting phase separation.* ***(C1)*** *TEM image and size distribution of Col-Au NPs from the supernatant.* ***(C2)*** *TEM image and size distribution of Col-Au NPs from the precipitate, showing aggregation and broad size distribution.*

Notably, the particle size remained constant with respect to both gelatin concentration and irradiation duration, in contrast to the previous findings. In Watari's chemical approach, increasing the gelatin concentration weakened electrostatic interactions between the positively charged amino groups of gelatin and the negatively charged Au NP surface, thereby modulating the metal core size. In the present case, the uniformity in particle size is attributed to the unique ablation dynamics of MCL-PLAL, particularly its short pulse duration, which promotes the formation of small, short-lived cavitation bubbles that limit the influence of matrix concentration on particle nucleation and growth. Furthermore, unlike the findings of Darroudi et al., there was no evidence of secondary ablation of preformed particles, suggesting the absence of fragmentation related size reduction in this system.

To evaluate the stability of the synthesized NPs and assess their suitability for potential biomedical applications, including cellular uptake and cytotoxicity, the hydrodynamic diameter of the Au:Gel colloids was analyzed using dynamic light scattering (DLS). Across the range of gelatin concentrations tested, the colloidal size remained largely consistent, with the exception of Entry 3 (Table 3), corresponding to the 0.1 wt% condition, where a noticeably smaller colloidal size was repeatedly observed.

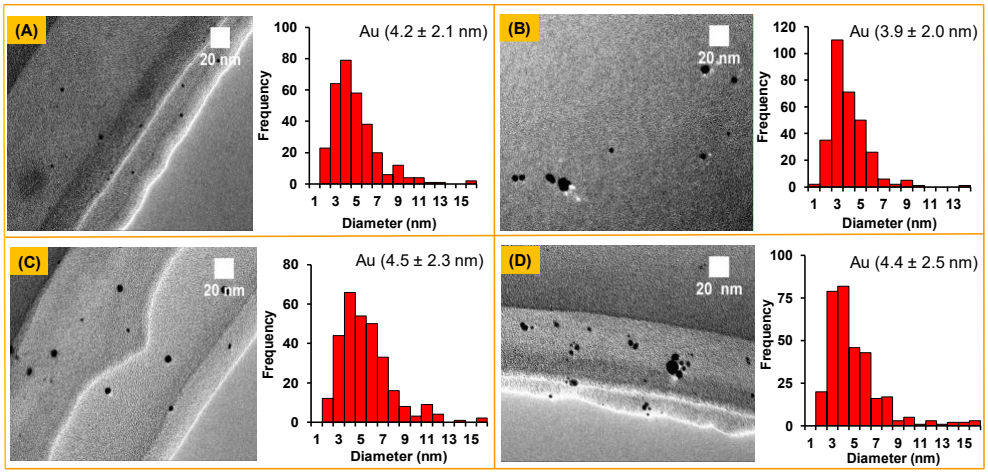

Figure 14 TEM micrographs and corresponding size distribution histograms of Au:Gel nanoparticles synthesized with different gelatin concentrations: 0.02% (A), 0.05% (B), 0.1% (C), and 0.5% (D). Scale bars represent 20 nm.

Prior to laser ablation, DLS measurements of gelatin solutions confirmed the immediate formation of colloidal structures, attributed to gelatin's amphiphilic nature. Interestingly, the size of these colloids was found to decrease linearly with increasing gelatin concentration. To further clarify whether colloidal dimensions, gelatin concentration, or AuNP yield were interdependent, inductively coupled plasma (ICP) spectroscopy was employed. The results confirmed that the particle size, gold content, and corresponding colloidal size were not correlated with gelatin concentration (Table 3). These results prove that MCL-PLAL process enables consistent nanoparticle formation regardless of matrix concentration.

Table 3 Effect of gelatin concentration on the characteristics of gold nanoparticles (Au:Gel NPs) synthesized via MCL-PLAL

Entry	Gel concentration (wt%)	Au:Gel NPs (nm)[a]	Yield of Au (mmol)[b]	Au:Gel colloid size (nm)[c]	Gel colloid size (nm)[c]
1	0.02	4.2 ± 2.1	4.4×10^{-5}	23 ± 4	11 ± 4
2	0.05	3.9 ± 2.0	5.7×10^{-5}	30 ± 4	7 ± 2
3	0.1	4.5 ± 2.3	2.2×10^{-5}	10 ± 4	7 ± 2
4	**0.2**	**4.3 ± 0.9**	**4.4×10^{-5}**	**31 ± 2**	**7 ± 1**
5	0.5	4.4 ± 2.5	7.5×10^{-5}	25 ± 3	4 ± 2

[a] is measured by TEM, [b] is measured by ICP, c is measured by DLS

To evaluate potential structural degradation of the gelatin matrix during nanoparticle formation, circular dichroism (CD) spectroscopy was employed, which is an established technique for probing the secondary structures of biomacromolecules. [18] CD measurements were conducted on both the Au:Gel nanocomposite and pristine gelatin solutions prepared at a concentration of 0.2 wt%. Both samples exhibited characteristic negative peaks at approximately 213 nm and 232 nm, [19,20] which are indicative of random coil conformations in the polypeptide chains. The CD spectrum of the Au:Gel sample closely resembled that of the native gelatin, displaying a broad negative band within the 200-300 nm range (Figure 15).

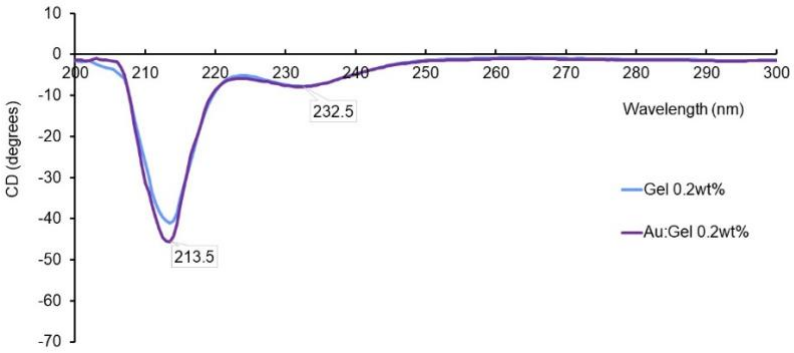

Figure 15 CD spectra of gelatin (0.2 wt%) before and after Au NP formation via MCL-PLAL.

The preservation of these spectral characteristics suggests that the random coil structure of gelatin was largely preserved following MCL-PLAL treatment at 0.2 wt%, indicating minimal damage to the protein's secondary structure under the applied conditions. To further investigate the possibility of chiral induction at the nanoparticle surface by the gelatin matrix, the CD spectral range was extended to 600 nm. However, no noticeable CD signals corresponding to the surface plasmon resonance (SPR) of AuNPs (typically observed between 500-600 nm) were detected (Figure 16). The absence of CD activity in this region implies that the gold nanoparticle surface did not undergo any chiral induction from the surrounding gelatin environment.

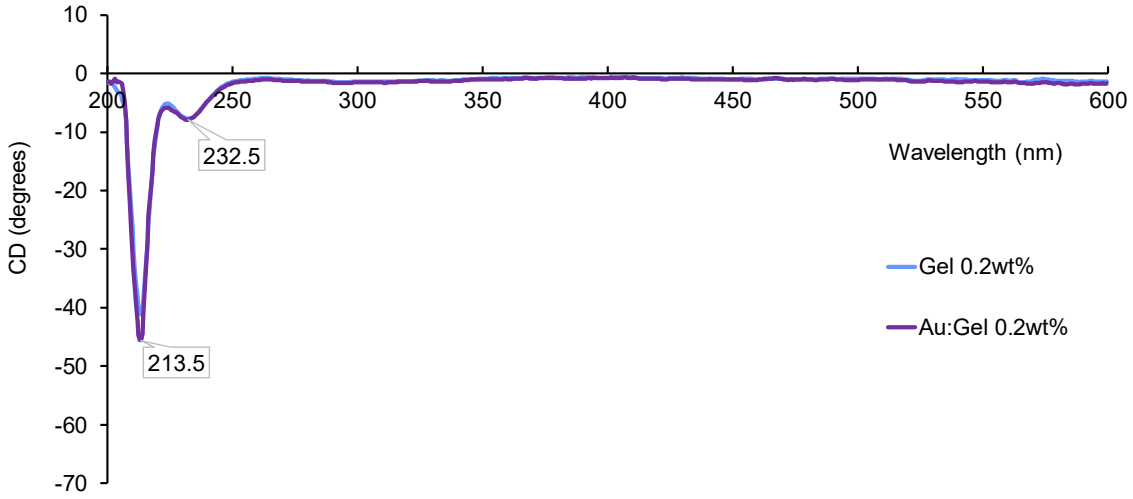

Figure 16 CD spectra of gelatin (0.2 wt%) before and after Au NP formation via MCL-PLAL at longer wavelength

In contrast, Au-Gel synthesized at a lower concentration of 0.02 wt% yielded different results. Under these conditions, gelatin displayed two clear negative peaks at 210 and 230 nm, which became more distinct. Additionally, a new positive peak appeared near 225 nm after laser ablation (Figure 17). This shift from the usual 232 nm signal observed in unmodified gelatin points to the formation of triple helical structures, resembling partially denatured native collagen.[21,22] Overall, the results indicate that MCL-PLAL modifies the secondary structure of gelatin, showing a more ordered conformation similar to collagen triple helices. This structural transformation could have potential advantages in materials science and biomedical fields. Altogether, the data show that MCL-PLAL can be used to adjust the gelatin structure depending on concentration, providing an effective method for creating nanocomposites with controlled bioactive conformations.

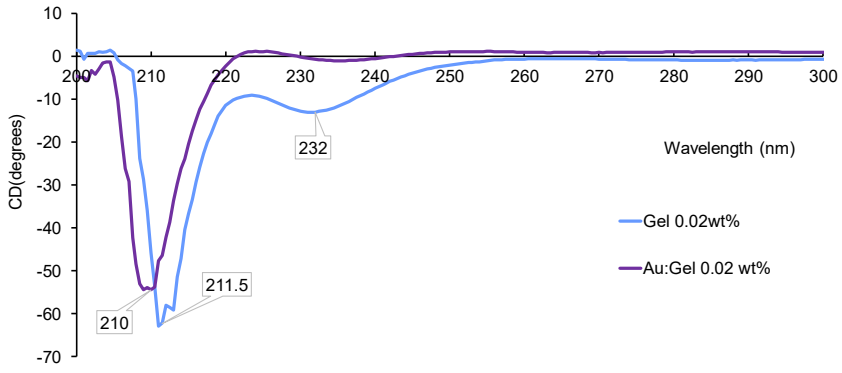

Figure 17 CD spectra of gelatin (0.02 wt%) before and after Au NP formation via MCL-PLAL.

Follow-up experiments investigated the impact of different media on impact of different media on reproducibility and Au-Gel NP synthesis. Using the optimized 0.2 wt% gelatin, phosphate-buffered saline (PBS) was tested to simulate cell culture conditions. Results (Table 4) showed no notable pH change in pure water, but PBS exhibited a substantial pH rise and solution turbidity, indicating salt involvement during ablation. Laser irradiation likely generated reactive species and altered phosphate ions, causing the pH shift. Additionally, PBS promoted Au NP aggregation over time, while aqua based samples remained stable, supporting water as the better medium for PLAL synthesis.

Table 4 Influence of matrix and solvent on pH, color, and gold yield after PLAL

Entry	Matrix	Concentration (wt%)	Solvent	pH before PLAL	pH after PLAL	Color after PLAL	ICP (mmol)
1	Gel	0.2	water	6.57	6.81	Clear red	4.4×10^{-5}
2	Gel	0.2	PBS	7.16	8.33	Cloudy red	3.8×10^{-6}
3	Col^I	0.2	PBS	6.57	6.81	Clear red	4.4×10^{-5}

Next, the author explored the direct synthesis of type I collagen (Col^I)-stabilized Au NPs using MCL-PLAL (Table 4, Entry 3). Unlike gelatin, Col^I does not form stable aqueous solutions without additives, requiring PBS despite its drawbacks. After one hour of irradiation, a faint pink supernatant and red precipitate indicated Au NP. Centrifugation separated the two phases for analysis. ICP-AES showed that 0.045 μmol of Au was ablated, with 94% in the precipitate. Due to Col^I s higher viscosity compared to water, ablation efficiency decreased, leading to lower AuNP yields. [26-28]

TEM analysis of the red precipitate confirmed AuNP formation, with a mean diameter of 16.6 ± 8.7 nm (Figure 13-C2). However, the precipitate could not be redispersed in water, suggesting Col^I deformation during ablation. In contrast, the supernatant, containing 6% of the total Au, had smaller and more uniform AuNPs averaging 2.4 ± 0.9 nm (Figure 13-C1), the smallest reported for Col^I matrices. [28]

2-4. Conclusions

In summary, the author has developed a method to directly incorporate Au NPs into sensitive biopolymer matrices using pulsed laser ablation in liquid (PLAL) with a microchip laser (MCL). This was done without a reducing agent. Despite the laser's low

pulse energy, the approach was highly efficient. It enabled the synthesis of gelatin-stabilized Au NPs averaging 4 nm, without damaging gelatin's structure. Meanwhile this is difficult to achieve with conventional methods. At low gelatin concentrations, the process also appeared to influence gelatin's secondary structure. Applying this method to type I collagen resulted in most Au NPs becoming trapped in the aggregated matrix, but a small fraction of well dispersed, small Au NPs was obtained. The lower yield may come from PBS degradation under laser irradiation, suggesting PBS should be avoided in future work. Overall, this MCL-PLAL method offers a distinct and promising strategy for synthesizing NPs under mild conditions in sensitive biological systems.

2-5. References

(1) Kogan, M.J.; Olmedo, I.; Hosta, L.; Guerrero, A.R.; Cruz, L.J.; Albericio, F. Peptides and Metallic Nanoparticles for Biomedical Applications. Nanomedicine **2007**, 2, 287–306.

(2) Khlebtsov, N.G.; Dykman, L.A. Optical Properties and Biomedical Applications of Plasmonic Nanoparticles. J. Quant. Spectrosc. Radiat. Transf. **2010**, 111, 1–35.

(3) Elahi, N.; Kamali,M.; Baghersad,M.H. Recent Biomedical Applications of Gold Nanoparticles: A Review. Talanta **2018**, 184, 537–556.

(4) Chatterjee, S.; Lou, X.Y.; Liang, F.; Yang, Y.W. Surface-Functionalized Gold and Silver Nanoparticles for Colorimetric and Fluorescent Sensing of Metal Ions and Biomolecules. Coord. Chem. Rev. **2022**, 459, 214461.

(5) Fatima, Z.; Saleem, R.; Khan, R.R.M.; Liaqat, M.; Pervaiz, M.; Saeed, Z.; Muhammad, G.; Amin, M.; Rasheed, S. Green Synthesis, Properties, and Biomedical Potential of Gold Nanoparticles: A Comprehensive Review. Biocatal. Agric. Biotechnol. **2024**, 59, 103271.

(6) Liu, X.; Luo, Y.; Zhang, Y.; Xie, Z.; Xu, C. Gold Nanoparticle-Mediated Fluorescence Resonance Energy Transfer for Analytical Applications in the Fields of Life Health and Safety. Talanta **2025**, 282, 127023.

(7) Kim, M.; Osone, S.; Kim, T.; Higashi, H.; Seto, T. Synthesis of Nanoparticles by Laser Ablation: A Review. KONA Powder Part. J. **2017**, 2017, 80–90.

(8) Balachandran, A.; Sreenilayam, S.P.; Madanan, K.; Thomas, S.; Brabazon, D. Nanoparticle Production via Laser Ablation Synthesis in Solution Method and Printed Electronic Application - A Brief Review. Results Eng. **2022**, 16, 100646.

(9) He, Y.; Wang, L.; Wu, T.; Wu, Z.; Chen, Y.; Yin, K. Facile Fabrication of Hierarchical Textures for Substrate-Independent and Durable Superhydrophobic Surfaces. Nanoscale 2022, 14, 9392–9400.

(10) Yin, K.; Wang, L.; Deng, Q.; Huang, Q.; Jiang, J.; Li, G.; He, J. Femtosecond Laser Thermal Accumulation-Triggered Micro-/Nanostructures with Patternable and Controllable Wettability Towards Liquid Manipulating. Nano-Micro Lett. **2022**, 14, 97.

(11) Darroudi, M.; Khorsand Zak, A.; Muhamad, M.R.; Zamiri, R. Preparation of Gelatinous Gold Nanoparticles by Pulsed Laser Ablation. Res. Chem. Intermed. **2015**, 41, 4587‑4594.

(12) Jiang, Z.; Li, L.; Huang, H.; He,W.; Ming,W. Progress in Laser Ablation and Biological Synthesis Processes: “Top-Down” and “Bottom-Up” Approaches for the Green Synthesis of Au/Ag Nanoparticles. Int. J. Mol. Sci. **2022**, 23, 14658.

(13) Lim, H.H.; Taira, T. Sub-Nanosecond Laser Induced Air-Breakdown with Giant-Pulse Duration Tuned Nd:YAG Ceramic Micro-Laser by Cavity-Length Control. Opt. Express **2017**, 25, 6302.

(14) Hettiarachchi, B.S.; Takaoka, Y.; Uetake, Y.; Yakiyama, Y.; Lim, H.H.; Taira, T.; Maruyama, M.; Mori, Y.; Yoshikawa, H.Y.; Sakurai, H. Uncovering gold nanoparticle synthesis using a microchip laser system through pulsed laser ablation in aqueous solution. Ind.Chem. Mater. **2024**, 2, 340‑347.

(15) Hettiarachchi, B.S.; Takaoka, Y.; Uetake, Y.; Yakiyama, Y.; Yoshikawa, H.Y.; Maruyama, M.; Sakurai, H. Mechanistic Study in Gold Nanoparticle Synthesis through Microchip Laser Ablation in Organic Solvents. Metals **2024**, 14, 155.

(16) Hettiarachchi, B.S.; Yakiyama, Y.; Sakurai, H. Tailoring Carbon-Encapsulated Gold Nanoclusters via Microchip Laser Ablation in Polystyrene Solution: Controlling Size, Structure, and Photoluminescent Properties. RSC Appl. Interfaces **2025**, 2, 772‑779.

(17) Neupane, M.P.; Lee, S.J.; Park, I.S.; Lee, M.H.; Bae, T.S.; Kuboki, Y.; Uo, M.; Watari, F. Synthesis of Gelatin-Capped Gold Nanoparticles with Variable Gelatin Concentration. J. Nanopart. Res. **2011**, 13, 491‑498.

(18) Miles, A.J.; Janes, R.W.; Wallace, B.A. Tools and methods for circular dichroism spectroscopy of proteins: A tutorial review. Chem. Soc. Rev. **2021**, 50, 8400‑8413.
(19) Gopal, R.; Park, J.S.; Seo, C.H.; Park, Y. Applications of Circular Dichroism for Structural Analysis of Gelatin and Antimicrobial Peptides. Int. J. Mol. Sci. **2012**, 13, 3229‑3244.
(20) Rub, M.A.; Asiri, A.M.; Khan, J.M.; Khan, R.H.; Din, K.-U. Interaction of Gelatin with Promethazine Hydrochloride: Conductimetry, Tensiometry and Circular Dichroism Studies. J. Mol. Struct. **2013**, 1050, 35‑42.
(21) Asil, S.M.; Narayan, M. Molecular Interactions between Gelatin-Derived Carbon Quantum Dots and Apo-Myoglobin: Implications for Carbon Nanomaterial Frameworks. Int. J. Biol. Macromol. **2024**, 264, 130416.
(22) Lee, S.; Jo, K.; Kim, S.;Woo, M.; Choi, Y.; Jung, S. Food Hydrocolloids. Food Hydrocoll. **2025**, 160, 110739.
(23) Correard, F.; Maximova, K.; Estève, M.A.; Villard, C.; Roy, M.; Al-Kattan, A.; Sentis, M.; Gingras, M.; Kabashin, A.V.; Braguer, D. Gold Nanoparticles Prepared by Laser Ablation in Aqueous Biocompatible Solutions: Assessment of Safety and Biological Identity for Nanomedicine Applications. Int. J. Nanomed. **2014**, 9, 5415‑5430.
(24) Levy, A.; De Anda Villa, M.; Laurens, G.; Blanchet, V.; Bozek, J.; Gaudin, J.; Lamour, E.; Mace, S.; Mignon, P.; Milosavljevic, A.R.; et al. Surface Chemistry of Gold Nanoparticles Produced by Laser Ablation in Pure and Saline Water. Langmuir **2021**, 37, 5783‑5794.
(25) Kwon, H.; Kim, K.K.; Song, J.K.; Park, S.M. The Effects of Ambient Ions on the Growth of Gold Nanoparticles by Laser Ablation in Liquid. Bull. Korean Chem. Soc. **2014**, 35, 865‑870.
(26) Costela, A.; Garcia-Moreno, I.; Barroso, J.; Sastre, R. Laser Performance of Coumarin 540A Dye Molecules in Polymeric Host Media with Different Viscosities: From Liquid Solution to Solid Polymer Matrix. J. Appl. Phys. **1998**, 83, 650‑660.
(27) Takata, T.; Enoki, M.; Chivavibul, P.; Matsui, A.; Kobayashi, Y. Effect of Confinement Layer on Laser Ablation and Cavitation Bubble during Laser Shock Peening. Mater. Trans. **2016**, 57, 1776‑1783.
(28) Hupfeld, T.; Laurens, G.; Merabia, S.; Barcikowski, S.; Gokce, B.; Amans, D. Dynamics of Laser-Induced Cavitation Bubbles at a Solid-Liquid Interface in High Viscosity and High Capillary Number Regimes. J. Appl. Phys. **2020**, 127, 044306.

Chapter 3

Transition Metal-chelated Collagen Hydrogels as a Template for the Metal Nanoparticles-encapsulated Elastic Gels by Gamma-ray Irradiation

Nazgul Assan, Yuta Uetake, Tomoyuki Suezawa, Rino Kamata, Michiya Matsusaki, Satoshi Seino, Hidehiro Sakurai

RSC Advances **2025,** *15*, 22824.

3-1. Introduction

The first report on metal nanoparticle (NP)-hydrogel composites was published by Willner et al.,[1] and they have gradually gained attention in materials science and applied chemistry.[2-5] Loh et al. later identified several important strategies for achieving uniformly dispersed NP-hydrogel systems:

- ❖ forming hydrogels in the presence of metal NP suspensions
- ❖ physically embedding metal NPs into hydrogels after gelation
- ❖ generating metal NPs within pre-formed gels
- ❖ using metal NPs as cross-linking agents during gel formation
- ❖ constructing gels from combinations of NPs, polymers, and specific gelator molecules.

These approaches have led to the development of a wide variety of NP-hydrogel composites designed for different functional purposes.[6] Collagen is one of the most widely explored polymer matrices for hydrogel precursors, primarily due to its excellent biocompatibility and biodegradability.[7-14] Combining collagen with functional synthetic polymers allows the introduction of new properties while maintaining its natural bioactivity. These hybrid materials have found broad applications in both biomedical fields and materials sciences.[15-17] Among the introduced functionalities, temperature sensitivity is especially valuable for drug delivery systems. [2] For example, Chmielewski et al. developed hydrogels based on collagen peptides and PEG that demonstrate thermo-responsive behavior.[7]

Biopolymers, such as collagen, are commonly used as stabilizing matrices for metal nanoparticles (NPs), helping to prevent their aggregation. Embedding metal NPs within polymer frameworks not only enhances their stability but also confers unique physicochemical characteristics to the resulting hydrogel, broadening its application potential. In 2008, Slowinska et al. introduced a crosslinked collagen hydrogel functionalized with tiopronin-capped gold nanoparticles (AuNPs) via a condensation reaction mediated by 1-(3-dimethylaminopropyl)-3-ethylcarbodiimide (EDC).[8,9,13] These collagen AuNP composites demonstrated favorable biodegradability and low cytotoxicity, making them promising candidates for drug delivery, photothermal therapy, imaging, and targeted cellular applications.[13] Beyond gold, collagen based composites incorporating other transition metals such as silver,[15, 16] iron oxide,[17, 18] chromium oxide (Cr_2O_3),[19]

gadolinium oxide (Gd_2O_3),[20] lanthanum oxide (La_2O_3),[21,22] and iron-doped zinc (Fe:Zn) [23] have also been developed.[24,25] However, most of these fabrication methods rely on pre-synthesized, surfactant-coated nanoparticles, which can lead to undesired chemical modifications of collagen and introduce residual contaminants.[26] An exception is the approach reported by Jiao, Zou, and Yan et al., who developed a method for creating collagen hydrogels containing Au NPs through electrostatic interactions between positively charged collagen and anionic gold complexes ($[AuCl_4]^-$), followed by biomineralization.[27,28] This technique eliminates the need for preformed nanoparticles, providing a more straightforward route to producing collagen Au NP hydrogel composites.

In a prior work in which the author was listed as a co-author, it was demonstrated that the addition of transition metal ions could rapidly and selectively induce gelation in collagen solutions, resulting in the formation of collagen-transition metal (Col-TM) gels (Scheme 3A).[29] For instance, introducing a solution of K_2PtCl_4 into purified type I collagen dissolved in phosphate-buffered saline (PBS) led to gelation through cross-linking between collagen fibers and Pt(II) ions, producing transparent and mechanically stable Col-Pt gels. This approach presents new opportunities for utilizing collagen in transparent gel systems for biomedical applications, such as 3D cell and organoid cultures. Based on this phenomenon, it was anticipated that converting Col-TM gels into collagen-transition metal nanoparticle (Col-TMNP) gels would yield materials with both desirable mechanical properties and added functionalities resulting from the embedded nanoparticles.

However, the rapid gelation initiated by metal ion addition creates difficulties for applying conventional solution-phase reduction methods to form nanoparticles within the gel. Moreover, previously explored strategies involving complexation and biomineralization proved ineffective for metal NP formation, as collagen lacks sufficient reducing power. To overcome this, the author has identified the need for a more versatile reduction technique that is not limited by the physical form of the material. Separately, the author has also developed a method to synthesize gold nanoparticles using microchip laser (MCL) ablation of bulk gold, which avoids metal-ion coordination entirely. Although this MCL approach efficiently generates gold NPs,[30] it still faces a challenge: the PBS buffer decomposes under laser ablation, causing nanoparticle aggregation. That

problem still remains unresolved.

In this context, the author has proposed employing radiochemical reduction as a strategy. Since the first reports on the radiochemical synthesis of metal nanoparticles, this technique has been regarded as a clean and efficient method, as it does not require chemical reducing agents.[31-34] It is also well established that nanoparticles produced via this route tend to be uniformly dispersed, due to reduction and nucleation processes, which can occur at the same time.[35] Additionally, high energy radiation sources like γ-rays and electron beams provide deep penetration, supporting the scalability of the synthesis. Based on these advantages, the author has hypothesized that reducing metal ions within Col-TM gels using radiochemical methods would facilitate in situ nanoparticle formation, resulting in Col-TMNP gels. This study presents the fabrication of Col-TMNP gels using γ-ray irradiation (Scheme 3B) and evaluate their elasticity and thermo-responsive behavior.

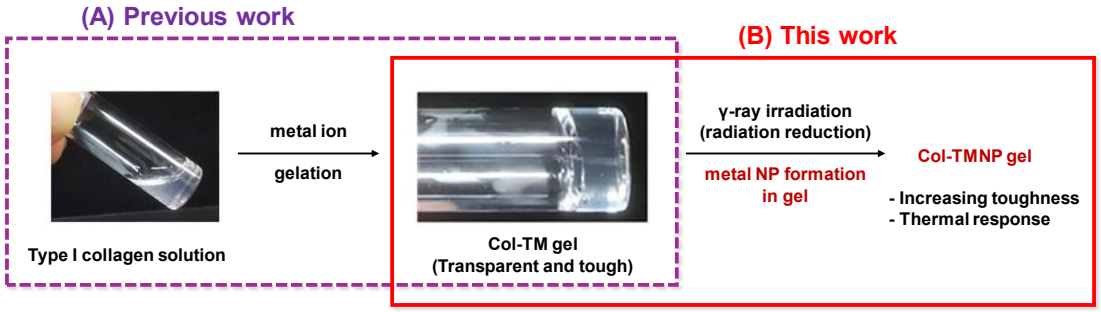

Scheme 3 Schematic comparison of previous and current work on collagen based gels.

3-2. Experimental section

3-2-1. Materials

Type I collagen (pepsin-treated, porcine skin) and unpurified collagen sponges were provided by NH Foods Ltd. Collagen nanofiber (CNF) solution in PBS was prepared following a published method. [29] PBS powder was purchased from Sigma-Aldrich and dissolved in water (pH 7.4). Acetic acid was from KISHIDA CHEMICAL, and ethanol (99.5%) and silver nitrate were purchased from Nacalai Tesque. Other chemicals, including gelatin, NaCl, Tris-HCl buffer, DMSO, acetone, n-hexane, $HAuCl_4 \cdot 3H_2O$, $K_2PtCl_4 \cdot 3H_2O$, $CuCl_2 \cdot 2H_2O$, $NiCl_2 \cdot 6H_2O$, and THF, were obtained from FUJIFILM Wako. $PdCl_2$ was sourced from Kanto Chemical, and $H_2PtCl_6 \cdot 6H_2O$ was purchased from Tanaka Kikinzoku Kogyo.

3-2-2. Preparation of Col-TMNP Gels

5 mL of 0.2 wt% CNF in PBS was placed in a vial. Then, 2.5 μmol of a metal ion solution was added to form a Col-TM gel. The vial was sealed and irradiated with γ-rays from a ^{60}Co source (Koga Isotope, Ltd.) with a total dose of ~20 kGy. The resulting Col-TMNP gel was collected for analysis. Gel shrinkage was assessed by measuring the change in volume.

3-2-3. TEM Sample Preparation

Transmission electron microscopy (TEM) was performed using a JEOL JEM-2100 at 200 kV. Holey carbon coated copper grids (EM Japan) were treated by glow discharge to improve hydrophilicity. The Col-TMNP gel was sliced into 1-5 mm pieces and placed on the grids, then dried in a vacuum oven at 60 °C for 24 hours. Particle size was analyzed from TEM images using ImageJ, averaging data from 300 particles.

3-2-4. SEM Sample Preparation

Scanning electron microscopy (SEM) was conducted using a JEOL JSM-6701F at 15 kV. Gels were freeze-dried for 4 days, coated with osmium using an HPC-30 coater, and imaged. SEM images were analyzed using JEOL PC-SEM software.

3-2-5. Compression Testing

Compression tests were done at room temperature using a SHIMADZU EZ-Test or AGS-20NX system. Gels were shaped into cylinders (6 mm diameter, 3-8 mm height), and the compression speed was set to 1 mm/min with a maximum force of 200 mN. Diameter and height were measured three times with a digital caliper, and elastic modulus was calculated from the 5-10% strain region of the stress-strain curve.

3-2-6. Swelling Ratio Measurement

Col-TMNP gels were freeze-dried (24 h) and weighed (W_{dry}). They were then immersed in 2 mL PBS for 24 h, gently blotted, and reweighed (W_{wet}). The swelling ratio was calculated as:

$$\boldsymbol{Swelling\ ratio} = \frac{W_{wet} - W_{dry}}{W_{dry}} \times 100\%$$

Each measurement was repeated four times, and the average value was reported.

3-2-7. Photothermal Activity

A thermocouple (K-type, HD-1400K) was inserted into the Col-TMNP gel and placed in the laser path. A 515 nm Yb:YAG laser (Spectra-Physics) was directed at the sample from 25 cm away, at 50 mW for 5 minutes. The temperature was recorded continuously during

and after laser exposure. This process was repeated twice, and the average of three independent runs was reported. The laser setup is shown in Figure 18.

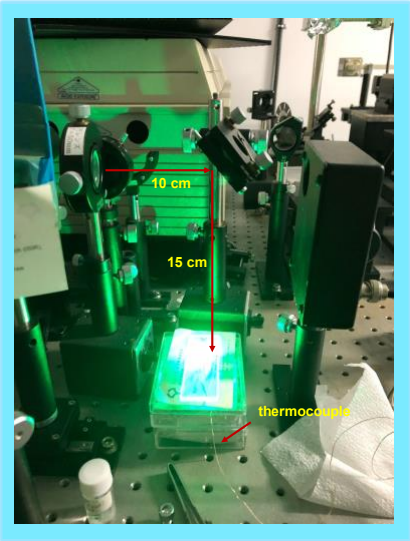

Figure 18 Laser set up for a photothermal experiment, 515 nm

3-3. Results and Discussions

The Col-Au gel was prepared following a previously established method, by mixing 0.2 wt% collagen nanofiber (CNF) solution with an aqueous $HAuCl_4$ solution (2.5 μmol) (Figure 19A). This gel was then subjected to γ-ray irradiation using a ^{60}Co source, delivering a total absorbed dose of approximately 20 kGy. After irradiation, the gel changed color from nearly colorless to reddish-brown, indicating the successful formation of gold nanoparticles (AuNPs) through surface plasmon resonance. Importantly, the gel retained its structure after irradiation, though its volume decreased to about 40% of its original size (Table 5). This shrinkage suggests that the crosslinking between CNFs via metal ions remained intact, while a portion of the water in the gel network was expelled.

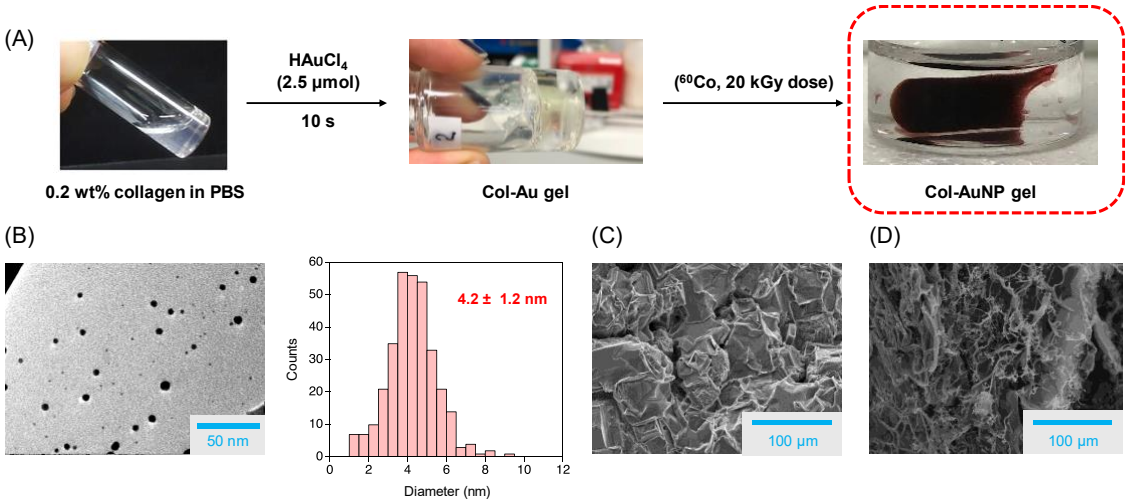

Figure 19 Synthesis and characterization of collagen–gold nanoparticle (Col–AuNP) gels via γ–ray irradiation. ***(A)*** *Schematic of the preparation process: 0.2 wt% collagen in PBS is mixed with $HAuCl_4$ to form a Col–Au gel, which is then irradiated with γ–rays generate the Col–Au NP gel.* ***(B)*** *TEM image and size distribution histogram of Au NPs, showing a mean diameter of 4.2 ± 1.2 nm.* ***(C, D)*** *SEM images of the Col–Au NP gel structure*

Transmission electron microscopy (TEM) analysis confirmed the presence of Au NPs with an average diameter of 4.1 ± 1.2 nm (Figure 19B). In contrast, TEM images of the pre-irradiated Col-Au gel showed no nanoparticles, verifying that NP formation occurred only after γ-ray exposure. When the pure collagen solution (without added gold) was irradiated under the same conditions, a shrunken gel also formed, but it was opaque and white, lacking the distinctive properties seen in the Col-Au NP gel.

Scanning electron microscopy (SEM) was also performed to observe structural differences between the gels. SEM images of the original Col-Au gel displayed a complex and uneven surface morphology (Figure 19C), whereas the Col-Au NP gel showed more clearly separated collagen fibers and a less complex structure (Figure 19D). These changes suggest that γ-ray irradiation may promote molecular level rearrangements within the collagen network, which could influence the mechanical properties of the resulting gel.

Building on the successful formation of Col-AuNP gels using γ-ray irradiation, the author extended this method to prepare Col-TMNP gels with other metals, including platinum, palladium, silver, nickel, and copper. Col-Pt gels, known for their mechanical strength, were synthesized using potassium tetrachloroplatinate (K_2PtCl_4) and hexachloroplatinic acid (H_2PtCl_6), followed by γ-ray exposure. These irradiations produced shrunken,

brownish gels that retained their gel-like consistency. TEM analysis confirmed the formation of platinum nanoparticles, with average sizes of 3.1 ± 1.6 nm for Pt(II) and 3.4 ± 1.2 nm for Pt(IV) systems (Table 5, entries 2 and 3). In the case of palladium, although the Col-Pd gel was initially formed by mixing collagen with H_2PdCl_4, the resulting Col-Pd NP gels became fragile and unsuitable for further testing after γ-ray treatment (entry 4). For silver, the addition of silver nitrate ($AgNO_3$) did not produce a Col-Ag gel due to the immediate formation of silver chloride precipitates, likely caused by residual chloride ions in the PBS buffer (entry 5). Nickel and copper systems, using $NiCl_2$ and $CuCl_2$ respectively, formed opaque white gels, and TEM results suggested little to no nanoparticle formation (entries 6 and 7). This is probably due to the higher redox potentials of Ni and Cu, which makes them harder to reduce compared to noble metals.

Interestingly, when non-purified collagen (containing both Type I and Type III collagen) was used instead of purified collagen, Col-Au NP gels still formed successfully. In this case, irradiation of a gel prepared with $HAuCl_4$ produced AuNPs with a particle size of 4.5 ± 1.5 nm (entry 8). On the other hand, gelatin, a denatured single chain form of collagen failed to form a gel either before or after γ-ray irradiation.

Table 5 Effect of different metal ions on nanoparticle size and gel shrinkage after gamma-ray irradiation

Entry	Metal ion	Size (nm)[b]	Shrinkage (%vol/vol)
1	$HAuCl_4$	4.1 ± 1.2	40
2	K_2PtCl_4	3.1 ± 1.6	44
3	H_2PtCl_6	3.4 ± 1.2	36
4	$PdCl_2$	–	–
5	$AgNO_3$	–	–
6	$NiCl_2$	–	35
7	$CuCl_2$	–	21
8[a]	$HAuCl_4$	4.5 ± 1.5	25

comment 1 a is done for Col(1+3 types), b is measured by TEM

3-3-1. Compression Experiment

The mechanical strength of the Col-TMNP gels was assessed through compression tests, and the results are shown in Figure 20A. The original Col-TM gels had relatively low elastic moduli: 2.5 kPa for Col-Au, 3.1 kPa for Col-Pt(II), and 1.9 kPa for Col-Pt(IV). In contrast, after γ-ray irradiation and nanoparticle formation, the Col-TMNP gels showed

significantly increased stiffness. Col-AuNP reached 10.1 kPa about five times greater than the original Col-Au gel. Similar improvements were seen for the platinum-based gels: Col-Pt(II)NP and Col-Pt(IV)NP showed increased moduli of 5.8 and 16.9 kPa, respectively. To determine whether these changes were statistically meaningful, two-tailed Student's t-tests were performed. The Pt(II) series did not show significant differences ($p > 0.05$), but the Au(III) ($p = 0.074$) and Pt(IV) ($p = 0.030$) series approached or met the commonly accepted threshold ($p \approx 0.05$), indicating meaningful improvements in mechanical properties. The observed stiffening and shrinkage of the gels are likely due to covalent crosslinking between collagen chains, initiated by radicals generated during γ-ray irradiation. Figure 20D outlines the proposed mechanism: radiolysis of water produces highly reactive species hydrated electrons (e_{aq}^-), hydrogen radicals (H•), and hydroxyl radicals (HO•) which are distributed uniformly throughout the gel due to the deep penetration of γ-rays. These species reduce metal ions to form nanoparticles and simultaneously create radicals on collagen molecules via hydrogen abstraction. These collagen radicals then form new covalent crosslinks (Figure 20E), increasing stiffness and compacting the gel matrix.

Although the specific role of ionic species in the original Col-TM gels is not fully understood, it is assumed that the initial metal-ligand coordination bonds are replaced by stronger covalent bonds during the reduction process. The resulting contraction of the gel is attributed to the closer packing of collagen chains due to these covalent linkages. Importantly, while the gel size decreased, its overall shape remained intact suggesting that metal ions initially served as a structural template during gel formation.

Further experiments using more concentrated collagen solutions revealed even higher stiffness in the resulting Col-TMNP gels. For example, Col-Pt(IV)NP prepared from concentrated collagen reached an elastic modulus of 88.3 kPa (Figure 20B). Statistical analysis confirmed the significance of these changes ($p < 0.05$). On the other hand, using purified versus unpurified collagen (containing both type I and type III) had no notable effect on the gel's stiffness (Figure 20C).

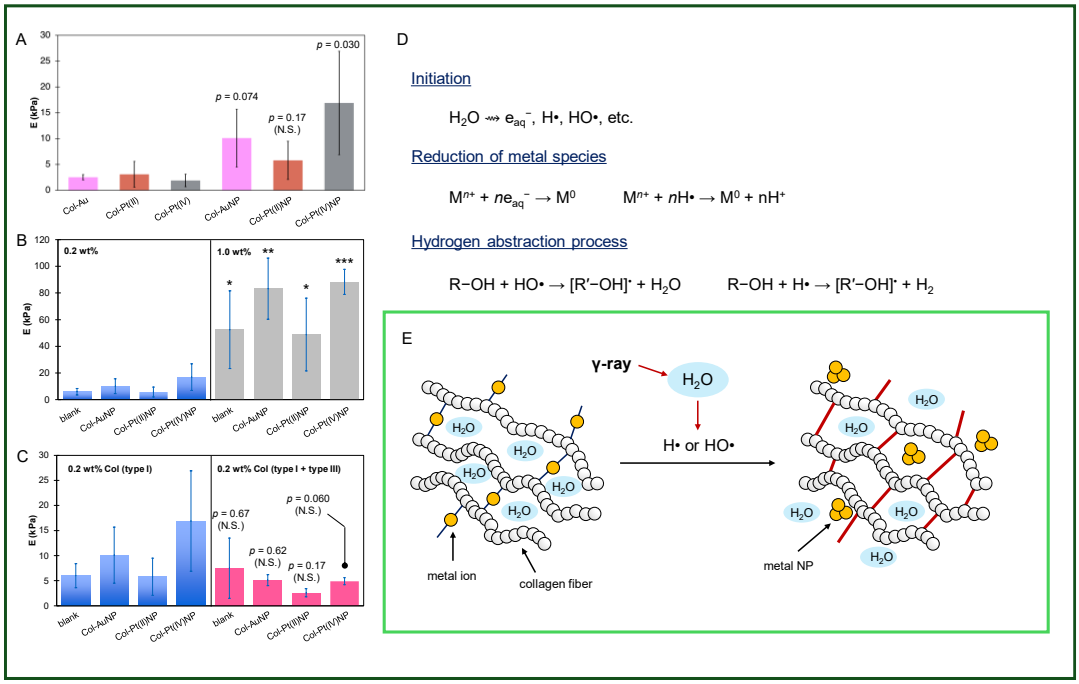

*Figure 20 Evaluation of elasticity and proposed mechanism of metal nanoparticle formation in collagen gels under γ-ray irradiation. Measurements (mean ± standard deviation) were based on four independent replicates (n=4). Statistical significance was determined using a two-tailed Student's t-test, with significance levels indicated as *p < 0.05, **p < 0.01, and ***p < 0.001; N.S. indicates no significant difference. (A) Comparison of Col-TMNP gels with Col-TM controls, with statistical tests performed relative to the corresponding Col-TM samples. (B) Influence of collagen concentration, analyzed against 0.2 wt% Col-TMNP as the reference group. (C) Influence of collagen purity. (D) Illustration of the radiochemical reaction pathways. (E) Schematic depiction of nanoparticle generation and radical induced crosslinking within collagen matrices.*

3-3-2. Swelling Ratio

To assess the water absorption capacity of the gels which influences their thermal and mechanical stability and ability to transport molecules the swelling behavior of Col-TMNP gels was measured. Freeze-dried Col-TMNP gels were soaked in PBS for 24 hours, and the swelling ratio was calculated. The irradiated collagen gel (without metal ions) showed a swelling ratio of 430% (Table 6). Interestingly, Col-TMNP gels had similar swelling ratios to the pure Col gel, indicating that the overall gel morphology especially pore size and the spacing between collagen chains is mainly shaped during the γ-ray irradiation step, not by the transition metal cross-linking.

However, the type of collagen used had a noticeable effect. Gels made with purified type I collagen showed significantly higher swelling than those made from mixed type I + III

collagen. Although the exact cause is unknown, this result suggests that type I collagen forms a more flexible network that absorbs more water.

When compared to previous studies, the swelling ratios observed here are relatively high. For example, Demeter et al.[36] reported about 250% swelling in electron beam-crosslinked collagen hydrogels, and Walimbe et al.[37] found much lower swelling (~35%) in hyaluronan-collagen gels, likely due to the stiffness added by collagen. In contrast, our Pt(IV)-containing Col-TMNP gels reached swelling ratios up to 690%. This differs significantly from Fu et al.'s report, where silver nanoparticles reduced swelling in collagen gels.[38]

These findings highlight that both the type of collagen and the specific nanoparticles embedded within the gel play crucial roles in determining water uptake. In particular, some metal nanoparticles such as Pt(IV) appear to increase gel flexibility and water-holding ability. Thus, by choosing appropriate metal nanoparticles and collagen types, it is possible to finely tune the swelling behavior of collagen based hydrogels. This opens up new opportunities for their use in applications like drug delivery, wound healing, and soft tissue engineering, where controlled swelling is essential.

Table 6 Swelling behavior for Col samples

Gel	Type I (%)	Type I + III (%)	*p*
Col gel	430 ± 194	360 ± 59	0.464
Col-AuNP	540 ± 87	410 ± 53	0.070
Col-Pt(IV)NP	490 ± 78	690 ± 64	0.063

3-3-3. Photothermal Activity of Au:Col and Pt:Col Gels

To explore the potential of Col-TMNP gels for practical use, the author further evaluated their photothermal behavior. Gels containing gold and platinum nanoparticles (Col-AuNP and Col-PtNP), as well as control Col gels without metal NPs, were subjected to photothermal experiments. Yb:YAG green laser (515 nm) with a power of 50 mW was used to irradiate the samples at room temperature. Each sample was exposed to the laser for 5 min, followed by a 5 min cooling period with the laser turned off. This heating and cooling cycle was repeated twice, and temperature changes were recorded throughout.

The results, shown in Figure 21, revealed that Col-AuNP gels experienced a temperature increase of 6 °C after 5 minutes of laser exposure. Col-PtNP gels showed a 3 °C rise, which is lower due to platinum's weaker light absorption compared to gold. Even the metal free Col gel showed a small increase of 1 °C, likely due to minor localized heating. Importantly, the temperature changes during the second cycle were nearly identical to the first, indicating good photothermal stability under the test conditions.

These findings are in line with previously reported studies. For example, Yang et al.[39] demonstrated that SiO_2@Au core-shell nanoparticles could raise temperatures by 4 to 9.7 °C under 532 nm laser irradiation, depending on gold cluster morphology. Their high photothermal efficiency was linked to strong near field interactions and uniform gold distribution. Jaque et al.[40] also emphasized that the composition and structure of nanoparticles significantly influence their photothermal performance.

Overall, the Col-AuNP gels in this study showed effective and stable photothermal conversion, making them promising candidates for biomedical applications such as photothermal therapy.

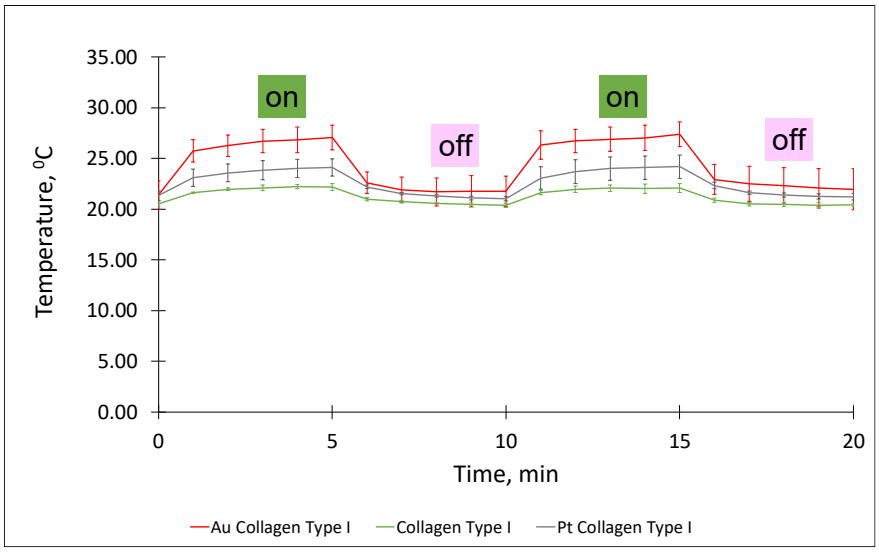

Figure 21 Time-dependent temperature profiles under Yb:YAG green laser irradiation (515 nm). Error bars represent standard deviations based on four independent measurements. Photothermal activity of newly prepared Col-TMNPs

3-4. Conclusions

In this study, a practical method for preparing collagen/metal nanoparticle (Col-TMNP) composite gels using a radiation-induced reduction approach was established. By incorporating transition metal ions such as gold and platinum, the author has successfully produced stiff collagen gels, with the elastic modulus reaching up to 88 kPa following γ-ray irradiation. This work was motivated by the challenges encountered in nanoparticle synthesis within collagen matrices using conventional solution-based reduction methods, where rapid gelation induced by metal ions prevented successful NP formation.[29]

To overcome this, the author turned her attention to γ-ray irradiation, a clean and versatile method that does not require chemical reducing agents and can be applied regardless of the material's physical form. The resulting process enables straightforward and contaminant-free fabrication of Col-TMNP gels.

The developed hydrogels demonstrated promising properties for applications in both biomedical and environmental areas. Very important functional characteristics, including mechanical strength, elasticity, swelling behavior, and photothermal response, were influenced by both the type of metal ion used and the preparation conditions. Significantly, γ-ray irradiation not only facilitated uniform nanoparticle synthesis but also triggered covalent crosslinking within the collagen network, improving stiffness and slightly reducing water absorption.

3-5. References

(1) Pardo-Yissar, V.; Gabai, R.; Shipway, A. N.; Bourenko, T.; Willner, I. Gold nanoparticle/hydrogel composites with solvent-switchable electronic properties. *Advanced Materials*, 2001, *13*(17), 1320-1323.

(2) Thoniyot, P.; Tan, M. J.; Karim, A. A.; Young, D. J.; Loh, X. J. Nanoparticle–Hydrogel Composites: Concept, Design, and Applications of These Promising, Multi-Functional Materials. Adv. Sci. 2015, 2 (1–2), 1–13. https://doi.org/10.1002/advs.201400010.

(3) Clasky, A. J.; Watchorn, J. D.; Chen, P. Z.; Gu, F. X. From Prevention to Diagnosis and Treatment: Biomedical Applications of Metal Nanoparticle-Hydrogel Composites. Acta Biomater. 2021, 122, 1–25. https://doi.org/10.1016/j.actbio.2020.12.030.

(4) Cha, G.D.; Lee, W.H.; Lim, C.; Choi, M.K.; Kim, D.-H. Materials engineering, processing, and device application of hydrogel nanocomposites. Nanoscale, 2020, 12(19), 10456-10473.

(5) Jeong, J.H.; Woo, H.C.; Kim, M.H. One-step green synthesis of 2D Ag-dendrite-embedded biopolymer hydrogel beads as a catalytic reactor. RSC advances 2021, 11(37), 22826-22834.

(6) Gazil, O.; Alonso Cerrón-Infantes, D.; Virgilio, N.; Unterlass, M. M. Hydrothermal Synthesis of Metal Nanoparticles@hydrogels and Statistical Evaluation of Reaction Conditions' Effects on Nanoparticle Morphologies. Nanoscale 2024, 16 (38). https://doi.org/10.1039/d4nr00581c.

(7) Pérez, C. M. R.; Rank, L. A.; Chmielewski, J. Tuning the Thermosensitive Properties of Hybrid Collagen Peptide-Polymer Hydrogels. Chem. Commun. 2014, 50 (60), 8174–8176. https://doi.org/10.1039/c4cc03171g.

(8) Castaneda, L.; Valle, J.; Yang, N.; Pluskat, S.; Slowinska, K. Collagen Cross-Linking with Au Nanoparticles. Biomacromolecules 2008, 9 (12), 3383–3388. https://doi.org/10.1021/bm800793z.

(9) Schuetz, T.; Richmond, N.; Harmon, M. E.; Schuetz, J.; Castaneda, L.; Slowinska, K. The Microstructure of Collagen Type I Gel Cross-Linked with Gold Nanoparticles. Colloids Surfaces B Biointerfaces 2013, 101, 118–125. https://doi.org/10.1016/j.colsurfb.2012.06.006.

(10) Poomrattanangoon, S.; Pissuwan, D. Gold Nanoparticles Coated with Collagen-I and Their Wound Healing Activity in Human Skin Fibroblast Cells. Heliyon 2024, 10 (13), e33302. https://doi.org/10.1016/j.heliyon.2024.e33302.

(11) Arun, A.; Malrautu, P.; Laha, A.; Ramakrishna, S. Gelatin Nanofibers in Drug Delivery Systems and Tissue Engineering. Eng. Sci. 2021, 16, 71–81. https://doi.org/10.30919/es8d527.

(12) Vo, Q. K.; Nguyen, A. T.; Ho, H. T.; Huynh, L. T. N.; Nguyen, T. P. P.; Nguyen, T. H. T. Environmentally Friendly Controlled Synthesis of Gold Nanostars with Collagen by One-Step Reduction Method. J. Nanomater. 2022, 2022. https://doi.org/10.1155/2022/4046389.

(13) Aminzai, M. T.; Patan, A. Recent Applications and Evaluation of Metal Nanoparticle-Polymer Hybrids as Chronic Wound Dressings. J. Nanomater. 2024, 2024. https://doi.org/10.1155/2024/3280349.

(14) Bîrcă, A.C.; Minculescu, M. A.; Niculescu, A.; Hudit, A.; Holban, A. M.; Alberts, A.; Grumezescu, A. M. Nanoparticle-Enhanced Collagen Hydrogels for Chronic Wound Management. 2025.

(15) Wu, H.; He, L.; Gao, M.; Gao, S.; Liao, X.; Shi, B. One-Step in Situ Assembly of Size-Controlled Silver Nanoparticles on Polyphenol-Grafted Collagen Fiber with Enhanced Antibacterial Properties. New J. Chem. 2011, 35 (12), 2902–2909. https://doi.org/10.1039/c1nj20674e.

(16) Mandal, A.; Sekar, S.; Chandrasekaran, N.; Mukherjee, A.; Sastry, T. P. Synthesis, Characterization and Evaluation of Collagen Scaffolds Crosslinked with Aminosilane

Functionalized Silver Nanoparticles: In Vitro and in Vivo Studies. J. Mater. Chem. B 2015, 3 (15), 3032–3043. https://doi.org/10.1039/c4tb02124j.
(17) Alliraja, C.; Rao, J. R.; Thanikaivelan, P. Magnetic Collagen Fibers Stabilized Using Functional Iron Oxide Nanoparticles in Non-Aqueous Medium. RSC Adv. 2015, 5 (27), 20939–20944. https://doi.org/10.1039/c4ra16181e.
(18) Mandal, A.; Dhineshkumar, E.; Murugan, E. Collagen Biocomposites Derived from Fish Waste: Doped and Cross-Linked with Functionalized Fe3O4 Nanoparticles and Their Comparative Studies with a Green Approach. ACS Omega 2023, 8 (27), 24256–24267. https://doi.org/10.1021/acsomega.3c01106.
(19) Sangeetha, S.; Ramamoorthy, U.; Sreeram, K. J.; Nair, B. U. Enhancing Collagen Stability through Nanostructures Containing Chromium(III) Oxide. Colloids Surfaces B Biointerfaces 2012, 100, 36–41. https://doi.org/10.1016/j.colsurfb.2012.05.015.
(20) Vijayan, V.; Kiran, M. S. Hybrid Nanostructured Gadolinium Oxide-Collagen-Dextran Polymeric Hydrogel for Corneal Repair and Regeneration. Int. J. Biol. Macromol. 2023, 224 (October 2022), 1423–1438. https://doi.org/10.1016/j.ijbiomac.2022.10.229.
(21) Vijayan, V.; Lakra, R.; Korrapati, P. S.; Kiran, M. S. Lanthanum Oxide Nanoparticle-Collagen Bio Matrix Induced Endothelial Cell Activation for Sustained Angiogenic Response for Biomaterial Integration. Colloids Surfaces B Biointerfaces 2022, 216 (October 2021), 112589. https://doi.org/10.1016/j.colsurfb.2022.112589.
(22) Vijayan, V.; Sreekumar, S.; Ahina, K. M.; Lakra, R.; Kiran, M. S. Lanthanum Oxide Nanoparticles Reinforced Collagen Κ-Carrageenan Hydroxyapatite Biocomposite as Angio-Osteogenic Biomaterial for In Vivo Osseointegration and Bone Repair. Adv. Biol. 2023, 7 (8), 1–19. https://doi.org/10.1002/adbi.202300039.
(23) Srivatsan, K. V.; Lakra, R.; Purna Sai, K.; Kiran, M. S. Effect of Bimetallic Iron:Zinc Nanoparticles on Collagen Stabilization. J. Mater. Chem. B 2016, 4 (8), 1437–1447. https://doi.org/10.1039/c5tb02047f.
(24) Vedhanayagam, M.; Kumar, A. S.; Nair, B. U.; Sreeram, K. J. Dendrimer-Functionalized Metal Oxide Nanoparticle-Mediated Self-Assembled Collagen Scaffold for Skin Regenerative Application: Function of Metal in Metal Oxides. Appl. Biochem. Biotechnol. 2022, 194 (1), 266–290. https://doi.org/10.1007/s12010-021-03764-w.
(25) S. Setoyama, R. Haraguchi, S. Aoki, Y. Oishi, T. Narita, *Int. J. Mol. Sci.* 2024, **25**, 10439.
(26) Pany, B.; Majumdar, A. G.; Bhat, S.; Si, S.; Yamanaka, J.; Mohanty, P. S. Polymerized Stimuli-Responsive Microgel Hybrids of Silver Nanoparticles as Efficient Reusable Catalyst for Reduction Reaction. Heliyon 2024, 10 (5), e26244. https://doi.org/10.1016/j.heliyon.2024.e26244.
(24) Xing, R.; Liu, K.; Jiao, T.; Zhang, N.; Ma, K.; Zhang, R.; Zou, Q.; Ma, G.; Yan, X. An Injectable Self-Assembling Collagen-Gold Hybrid Hydrogel for Combinatorial Antitumor Photothermal/Photodynamic Therapy. Adv. Mater. 2016, 28 (19), 3669–3676. https://doi.org/10.1002/adma.201600284.
(28) Tohidi, H.; Maleki, N.; Simchi, A. Conductive, Injectable, and Self-Healing Collagen-Hyaluronic Acid Hydrogels Loaded with Bacterial Cellulose and Gold Nanoparticles for Heart Tissue Engineering. Int. J. Biol. Macromol. 2024, 280 (P2), 135749. https://doi.org/10.1016/j.ijbiomac.2024.135749.
(29) Suezawa, T.; Sasaki, N.; Assan, N.; Uetake, Y.; Onuma, K.; Sakurai, H.; Katayama, R.; Inoue, M.; Matsusaki, M. Science Advances. 2023, 1–31.
(30) N. Assan, T. Suezawa, Y. Uetake, Y. Yakiyama, M. Matsusaki, H. Sakurai, *Colloids Interfaces* 2025*,* **9***,* 42.
(31) Belloni, J. Nucleation, Growth and Properties of Nanoclusters Studied by Radiation Chemistry: Application to Catalysis. Catal. Today 2006, 113 (3–4), 141–156. https://doi.org/10.1016/j.cattod.2005.11.082.
(32) Yang, Y.; Johansson, M.; Wiorek, A.; Tarakina, N. V.; Sayed, F.; Mathieu, R.; Jonsson, M.; Soroka, I. L. Gamma-radiation induced synthesis of freestanding nickel nanoparticles. Dalton Transactions, 2021, 50(1), 376-383.

(33) Yang, Y.; Montserrat-Sisó, G.; Wickman, B., Nikolaychuk, P. A.; Soroka, I. L. Core–shell and heterostructured silver–nickel nanocatalysts fabricated by γ-radiation induced synthesis for oxygen reduction in alkaline media. Dalton Transactions, 2022, 51(9), 3604-3615.

(34) Wang, Y.; Zhang, M.; Yan, Z.; Ji, S.; Xiao, S.; Gao, J. Metal Nanoparticle Hybrid Hydrogels: The State-of-the-Art of Combining Hard and Soft Materials to Promote Wound Healing. Theranostics 2024, 14 (4), 1534–1560. https://doi.org/10.7150/thno.91829.

(35) Seino, S.; Kinoshita, T.; Nakagawa, T.; Kojima, T.; Taniguci, R.; Okuda, S.; Yamamoto, T. A. Radiation Induced Synthesis of Gold/Iron-Oxide Composite Nanoparticles Using High-Energy Electron Beam. J. Nanoparticle Res. 2008, 10 (6), 1071–1076. https://doi.org/10.1007/s11051-007-9334-3.

(36) Demeter, M.; Călina, I.; Scărișoreanu, A.; Micutz, M.; Kaya, M. A. Correlations on the Structure and Properties of Collagen Hydrogels Produced by E-Beam Crosslinking. Materials (Basel). 2022, 15 (21), 1–15. https://doi.org/10.3390/ma15217663.

(37) Walimbe, T.; Calve, S.; Panitch, A.; Preeti, M.; Sciences, H.; Lafayette, W. HHS Public Access. 2020, No. 530, 97–107. https://doi.org/10.1016/j.actbio.2019.01.058.Incorporation.

(38) Wu, H.; He, L.; Gao, M.; Gao, S.; Liao, X.; Shi, B. One-step in situ assembly of size-controlled silver nanoparticles on polyphenol-grafted collagen fiber with enhanced antibacterial properties. New Journal of Chemistry, 2011, 35(12), 2902-2909.

(39) Yang L.; Yan, Z.; Yang, L.; Yang, J.; Jin, M.; Xing, X.; Zhou, G.; L. Shui, L. Photothermal Conversion of SiO2@Au Nanoparticles Mediated by Surface Morphology of Gold Cluster Layer. RSC Adv. 2020, 10, 33119. https://doi.org/10.1039/d0ra06278b.

(40) Jaque, D.; Martínez Maestro, L.; Del Rosal, B.; Haro-Gonzalez, P.; Benayas, A.; Plaza, J. L.; Martín Rodríguez, E.; García Solé, J. Nanoparticles for Photothermal Therapies. Nanoscale 2014, 6 (16), 9494–9530. https://doi.org/10.1039/c4nr00708e.

Concluding Remarks

This doctoral work has established a foundation for the design and synthesis of biopolymer-stabilized metal nanoparticles, with particular focus on integrating gold (Au) and platinum (Pt) nanoparticles into chitosan and collagen-based matrices.

The research systematically explored three distinct synthesis strategies matrix-transfer on chitosan, pulsed laser ablation in liquid with gelatin and collagen, and γ-ray induced radiochemical reduction within collagen hydrogels. Each of these approaches offered unique advantages for nanoparticle incorporation under mild, biocompatible conditions.

It has been demonstrated that even structurally sensitive biomaterials, such as gelatin and collagen, can successfully host metal nanoparticles without compromising their native properties. The study highlighted how mild, surfactant-free, and reducing-agent-free approaches can yield well-dispersed nanoparticles while preserving or enhancing the functional characteristics of the biopolymer matrices in the MCL-PLAL method.

Meanwhile, the γ-ray irradiation technique enabled the one-pot formation of metal nanoparticles and covalent crosslinking of collagen networks, producing robust hydrogels with tunable mechanical, optical, and photothermal properties.

Altogether, this research contributes to the growing field of hybrid nanomaterials by providing practical and sustainable strategies for synthesizing metal nanoparticle-biopolymer composites. These findings could pave their ways for future applications in biomedicine, soft robotics, sensing technologies, and environmental remediation. All these areas where the synergy between inorganic nanostructures and natural polymers hold immense promise.

List of publications

1. Size-selective Preparation of Gold Nanoparticles Stabilized on Chitosan Using the Matrix-Transfer Method.
Nazgul Assan, Yuta Uetake, Hidehiro Sakurai
Journal of Nanoparticle Research **2023**, *25*, 50.
DOI: 10.1007/s11051-023-05700-x

2. Exploring the Feasibility of a Microchip Laser Ablation Method for the Preparation of Biopolymer-Stabilized Gold Nanoparticles: Case Studies with Gelatin and Collagen.
Nazgul Assan, Tomoyuki Suezawa, Yuta Uetake, Yumi Yakiyama, Michiya Matsusaki, Hidehiro Sakurai
Colloids and Interfaces **2025**, *5*, 42.
DOI: 10.3390/colloids9040042

3. Increasing Stiffness and Thermal Response Behavior of Collagen/Metal Nanoparticles Composite Hydrogels Fabricated Through Radiochemical Reduction.
Nazgul Assan, Yuta Uetake, Tomoyuki Suezawa, Rino Kamata, Michiya Matsusaki, Satoshi Seino, Hidehiro Sakurai
RSC Advances **2025,** *15*, 22824.
DOI: 10.1039/D5RA03384E

List of Supplementary Publications:
4. Ultra-Rapid and Specific Gelation of Collagen Molecules for Transparent and Tough Gels by Transition Metal Complexation.
Tomoyuki Suezawa, Naoko Sasaki, Yuichi Yukawa, **Nazgul Assan**, Yuta Uetake, Kunishige Onuma, Rino Kamada, Daisuke Tomioka, Hidehiro Sakurai, Ryohei Katayama, Masahiro Inoue, Michiya Matsusaki
Advanced Science **2023**, *10*, 2302637.
DOI: 10.1002/advs.202302637

Acknowledgements

I would like to express my sincere appreciation to Professor Hidehiro Sakurai for being my graduate school supervisor both in master and PhD for the last 7 years. Words cannot fully express my deep gratitude for Professor Sakurai's patience, guidance, and unwavering belief in my research abilities despite the difficulties that I encountered during my studies in Osaka.

I am also deeply grateful to Associate Professor Yumi Yakiyama for her constant support through every lab report, presentation trial, conference, and in life overall. I cannot express enough appreciation for her consistent encouragement and personal support.

I would like to express my profound thanks to Assistant Professor Yuta Uetake for his constant support in manuscript writing, valuable recommendations, and non-stop editing of all of my manuscripts, without which I would not be able to get my PhD.

I had the great pleasure of working with Professor Michiya Matsusaki and Associate Professor Satoshi Seino, as both provided me with many starting materials, instrumentation facilities, and helped clarify my experimental data.

Furthermore, I would like to thank all the previous and current members of Sakurai Laboratory, especially Dr.Sitanan Sartyoungkul (my Anna), Dr.Artur Kasprzak, Ms.Michiko Ebukuro, Mr.Han Junyi, Dr.Barana Hettiarachchi, Dr.Peerapong Chumkaeo (Jojo), Dr.Threeraphat Chutimasakul (Champ), Dr.Butsaratip Suwattananuruk **(**Peet), Ms.Svetlana Em, Ms.Yuka Motohashi, Mr.Takumi Hasegawa, Dr. Maiki Nishimoto, Dr. Hironobu Nakazawa, Dr. Minghong Li, Ms. Mio Nishimura **(**Mio-chan), Mr. Katsuaki Iwasa and Mr. Shinji Kubota **(**Kubo-chan).

I separately would like to acknowledge my friends – Ms.Zhanar Kassenova (Zaichik), Dr.Leticia Sarmento, Ms.Kamshat Umbetova (Kama), Dr.Zarina Davletzhanova, Mr.Kyle Leinweber, Dr.Manunya Tepakidareekul (Kimmie) and Dr.Adam Ferry for their constant moral support. I am grateful to my Kazakhstani colleagues Dr. U.Bakhbergen, Dr. N.Khan, and Dr. N.Baikalov whose friendship and support were invaluable throughout the course of my work.

I would like to extend my thanks to my parents Dr. Assan Zhexembayev and Mrs. Gainizhamal Zhexembayeva, my sisters, all of my nephews, my son – Abish Assan, because without their support I have never thought enduring this career path.

Finally, I would like to say thanks for government of Japan for their Monbukagakusho: MEXT scholarship and The University of Osaka for giving me a life-changing opportunity to study and do research.

July 2025

Nazgul Assan